PSERC

Voltage Security Margin Assessment

Final Project Report

Power Systems Engineering Research Center

A National Science Foundation
Industry/University Cooperative Research Center
since 1996

Power Systems Engineering Research Center

Voltage Security Margin Assessment

Final Project Report

Project Team

Garng M. Huang
Ali Abur
Texas A&M University

PSERC Publication 02-49

December 2002

Information about this Project

For information about this project contact:

Garng M. Huang
Professor
Electrical Engineering Department
Texas A&M University
College Station, TX 77840
Phone: 979-845-7476
Email: huang@ee.tamu.edu

Power Systems Engineering Research Center

This is a project report from the Power Systems Engineering Research Center (PSERC). PSERC is a multi-university Center conducting research on challenges facing a restructuring electric power industry and educating the next generation of power engineers. More information about PSERC can be found at the Center's website: http://www.pserc.wisc.edu.

For additional information, contact:

Power Systems Engineering Research Center
Cornell University
428 Phillips Hall
Ithaca, New York 14853
Phone: 607-255-5601
Fax: 607-255-8871

Notice Concerning Copyright Material

ACKNOWLEDGEMENTS

The work described in this report was sponsored by the Power Systems Engineering Research Center (PSERC). We express our appreciation for the support provided by PSERC's industrial members and by the National Science Foundation under grant NSF EEC-0002917 received under the Industry / University Cooperative Research Center program.

The industry advisors for the project were Mani Subramanian, ABB Network Management; Don Sevcik, CenterPoint Energy; and Bruce Dietzman, Oncor. Their suggestions and contributions to the work are appreciated.

EXECUTIVE SUMMARY

Increasingly, within restructured power systems, voltage stability issues are becoming significant in the way we plan, operate and maintain the system. The involvement of new players in the electricity power business has led to the proliferation of intra-area and inter-area transactions of electricity in the transmission network. Typically, these transactions are of considerably shorter duration and larger variety than that in a vertically-integrated utility (VIU) structure where a single utility controls power generation, transmission and distribution within a given area. Not only does this new operating environment lead to frequent and significant changes in system operating points and load flow patterns, but it also results in increasing volatility in system conditions. This leads to potential security and reliability degradation in system operations, such as in voltage stability.

There is a need to evolve procedures that insure voltage stability in the operation of more open and diverse power systems. To achieve this aim, power system operators need to be able to quickly assess from measurable quantities, the operational state of the system from the voltage stability perspective. At the same time, in case of stability problems, the responsibility evaluation procedures need to be distinctly identified within the new operating environment.

The objective of this project was to evolve a framework, within the context of the restructured power market operations, to incorporate voltage stability assessment into the power system security, accountability and utilization factors for control devices. In the course of completing the objective of this project, we have come up with new and practical algorithms and procedures that can effectively address the incorporation of voltage stability into market-oriented power system operations. We summarize the significant outcomes of our work as given below.

- Dynamic modeling of generators, governors, ULTC, switched capacitor and loads using EUROSTAG has been carried to study dynamic voltage stability and the importance of dynamic reserves to maintain stability [8]. Detecting dynamic voltage collapse using state information has been investigated for a variety of dynamic disturbances [4]. Static modeling of FACTS devices in investigating voltage stability studies also has been carried out. It is observed that usage of devices such as TCSC and SVC could improve stability margin significantly [3].

- A new way of using bifurcation analysis, using the unreduced Jacobian matrix [7] that avoids singularity induced infinity problem and is computationally attractive, has been formulated.

- Within the context of an open power market, the responsibility evaluation of a potential voltage collapse assumes significance. Using bifurcation analysis, a procedure to allocate contribution of generators, transmission and control elements in voltage stability has been evolved [6]. This could be used as the basis for evaluating the utilization factors and the pricing of control elements in a power system.

- An algorithm to compute Optimal Power Flow incorporating voltage stability has been proposed [1]. The voltage stability constraint is computed from the power flow state variables and the network topology. This algorithm has been applied further to evaluate reliability indices in planning stages [2]. The incorporation of voltage stability enhancement devices (such as FACTS devices) into the algorithm has also been formulated [3].

- The framework for transaction-based power flow analysis for transmission utilization allocation has been proposed [10]. The methods to model transactions for both pool type and point-to-point long-term bilateral type transaction have been designed. This analysis has been used to address the approach to equitable loss allocation in a competitive market [11]. The approach has been applied to congestion management and responsibility evaluation in such a market [9].

- A new way to evaluate voltage stability responsibility in a composite market model framework, having both the pool type spot market and the bilateral long-term transactions, has been devised [5]. This decomposition approach has the potential to address voltage stability usage, voltage security pricing and responsibility settlement in a transaction-based power market.

TABLE OF CONTENTS

TABLE OF CONTENTS (continued)

1
Voltage Stability Studies and Modeling Issues

1.1 Typical two-bus system for voltage stability studies

We have taken a sample two-bus system that is generally used to study the basic phenomenon of static voltage stability. The following subsections give details of our analysis and simulations.

The model for studying voltage stability, a generator supplying a constant power load through a transmission line, is shown in Figure 1-1.

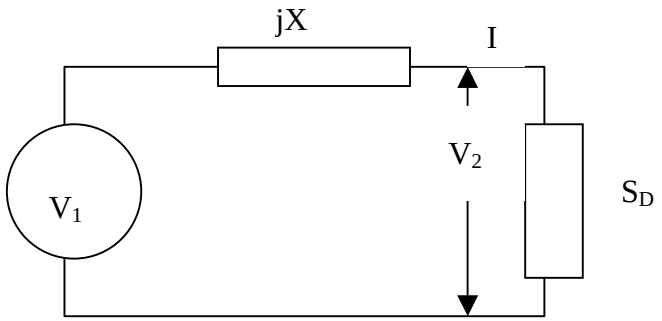

Figure 1-1 Two-bus representation model

From the figure,

$$\begin{aligned} S_D &= V_2 I^* \\ &= |V_2 I| e^{j\phi} \\ &= |V_2 I| (\cos\phi + j \sin\phi) \\ &= P_D (1 + j\beta) \end{aligned}$$

where $\beta = \tan\phi$.

Now we know that,

$$P_D = -P_{21} = P_{12} = \frac{|V_1 V_2|}{X} \sin\theta_{12}$$

$$Q_D = -Q_{21} = Q_{12} = \frac{|V_1 V_2|}{X} \cos\theta_{12} - \frac{|V_1|^2}{X}$$

Eliminating θ_{12} and solving the second order equation we finally get,

$$|V_2|^2 = \frac{|V_1|^2}{2} - \beta P_D X + \left[\frac{|V_1|^4}{4} - P_D X (P_D X + \beta |V_1|^2) \right]^{1/2} \quad (1.1)$$

As seen from equation (1.1), the voltage at the load point is influenced by the power delivered to the load, the reactance of the line, and the power factor of the load. The voltage has two solutions; the higher one is the stable solution. The load at which the two solutions have one value indicates the steady state voltage collapse point. This is also reflected in the eigenvalue analysis of the Jacobian matrix as an eigenvalue approaches zero, which will be discussed in detail later on.

1.1.1 Test system used for simulation

The test system used in our simulation is shown in Figure 1-2, which generalizes the system in Figure 1-1 by associating components with physical devices. The generator control will be analyzed more in Chapter 6. The transmission control block is representative of devices like TCSC's (Thyristor Controlled Series Capacitors) and SVC's (Static VAR Compensators). The voltage at the generator bus, E, is taken as 1.0 p.u. The reactance of the line is taken to be 0.15 p.u.

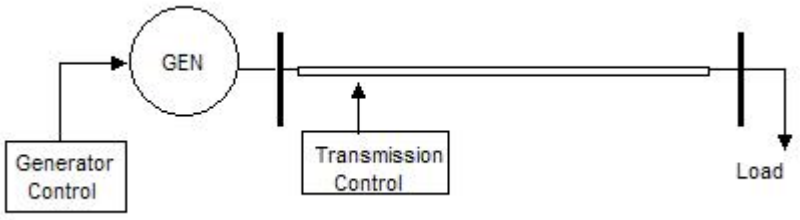

Figure 1-2 Test system

1.1.2 Effects studied

Our first effort was to study the effect of various control apparatuses (such as TCSC's and SVC's) and load conditions (such as power factor and nature of the loads) on the steady state voltage stability. The cases we have simulated are:

1) Effect of power factor
2) Effect of TCSC
3) Effect of SVC
4) Effect of SVC position
5) Effect of type of loading.

1.1.3 Software used for simulation

We have used a MATLAB-based program for repeated power flows, with increased loading at the load bus, to study voltage stability. At the collapse point, the load flow program would fail to converge and give a solution.

For SVC and loading-type impact studies on voltage stability, we have used EUROSTAG for simulations.

1.2 Power factor issues on static voltage collapse limits

It can be seen from the Figure 1-3 that as the power factor degrades (i.e., comes down), the voltage collapse occurs at lower power delivery.

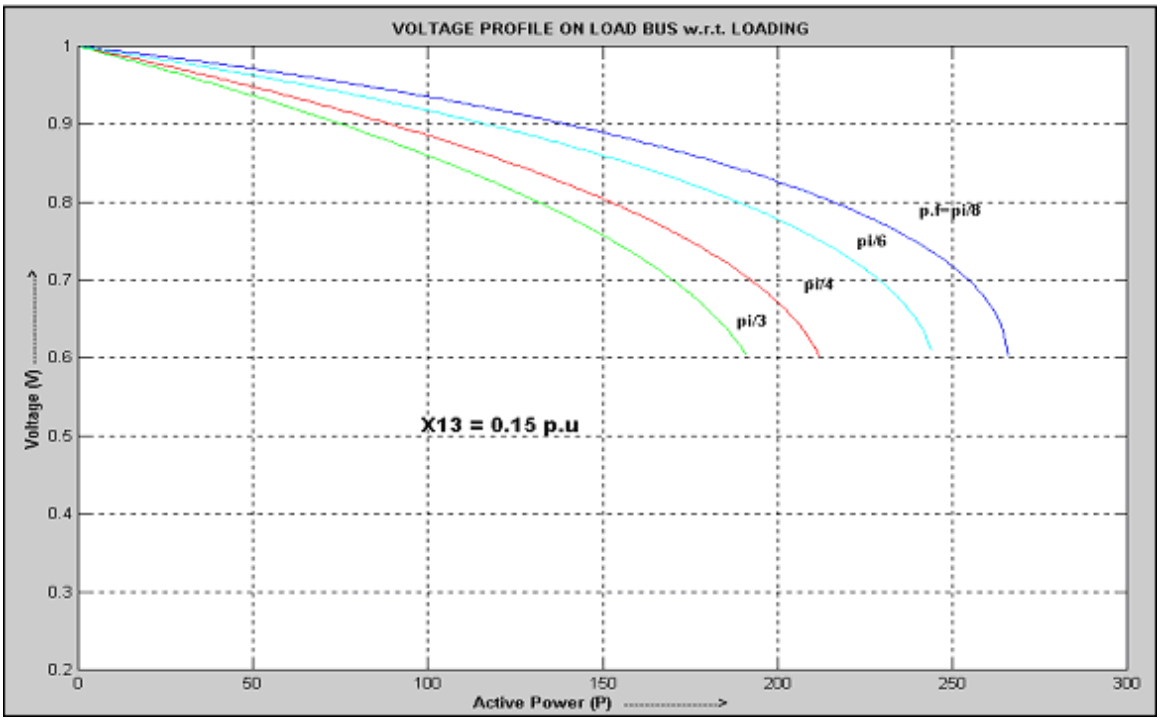

Figure 1-3 Effect of power factor on voltage collapse

1.3 Modeling of TCSC and its effect on static voltage stability analysis

A TCSC is a control device that is installed in the line to control the line impedance thereby controlling the maximum power loading in the lines. Generally, one can control the line impedance up to $\pm 50\%$ using the TCSC. As far as steady state voltage stability analysis is concerned, we can model TCSC as a variable capacitor in series with the line impedance.

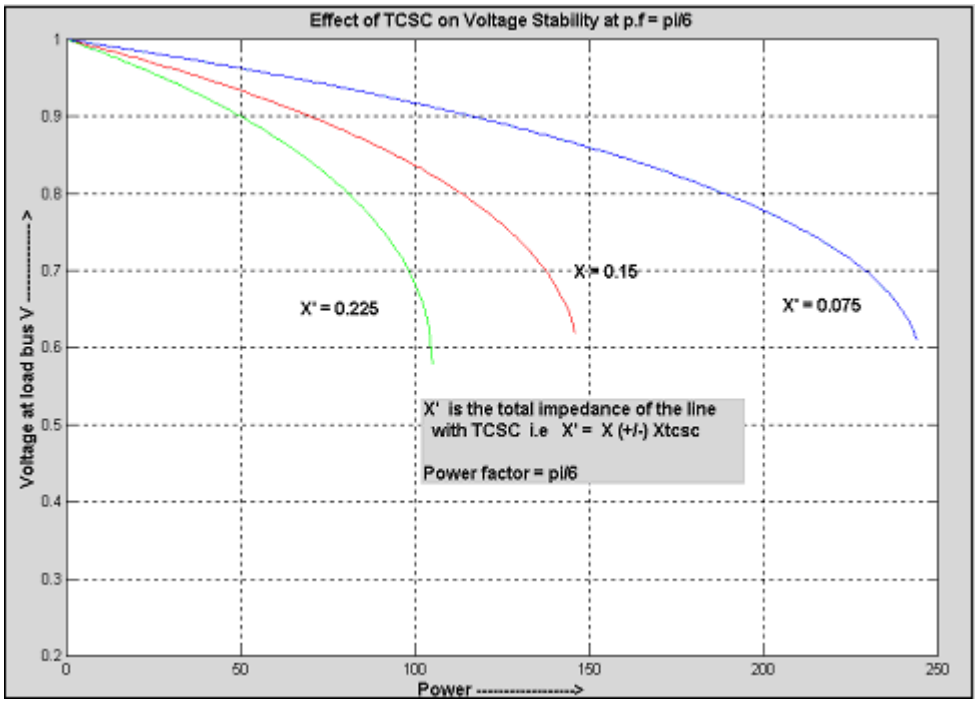

Figure 1-4 Effect of TCSC on voltage stability

It can be seen in Figure 1-4 that the lower the line impedance, the higher the voltage collapse point. Hence, it can be inferred that by employing TCSC's to reduce line impedance for long lines, one can increase the voltage stability margin at the load end of the lines.

1.4 Modeling of SVC and its effect on voltage stability analysis

SVC's provides voltage support to the line. A SVC is modeled as a PV bus with zero real power in the power flow analysis. It is observed from Figure 1-5 that by employing a SVC at the middle of the line (i.e., supporting voltage in between the generation and load buses), one can improve the voltage stability margin at the load end. Moreover, by placing two SVC's at equal distance between the buses, the collapse point increases further as shown in Figure 1-6.

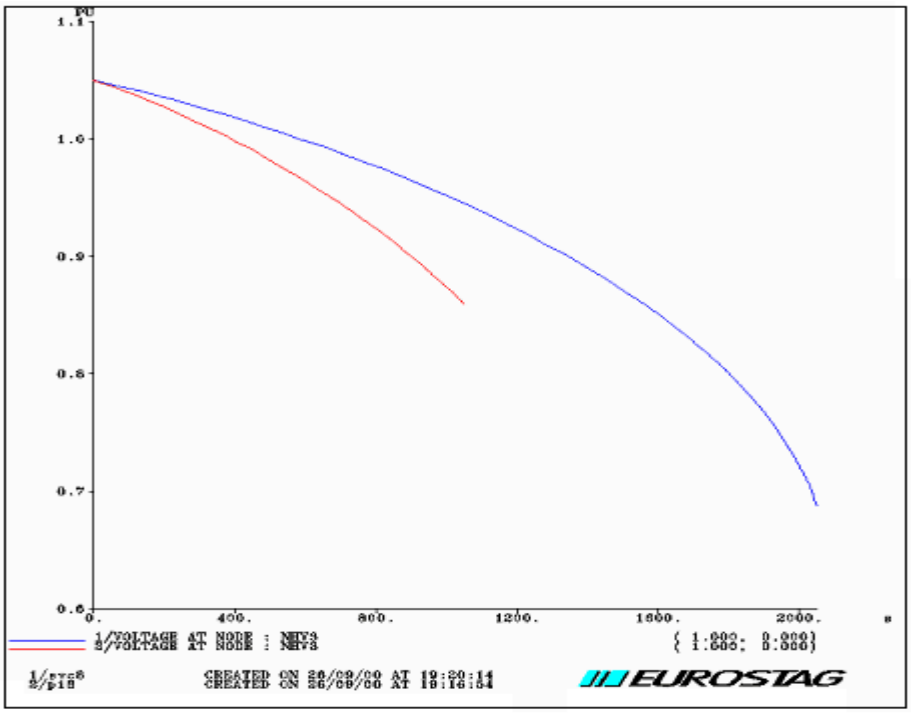

Figure 1-5 Effect of SVC on voltage stability. Top curve represents voltage with a SVC at the middle of the transmission line. The bottom curve gives the voltage profile without a SVC.

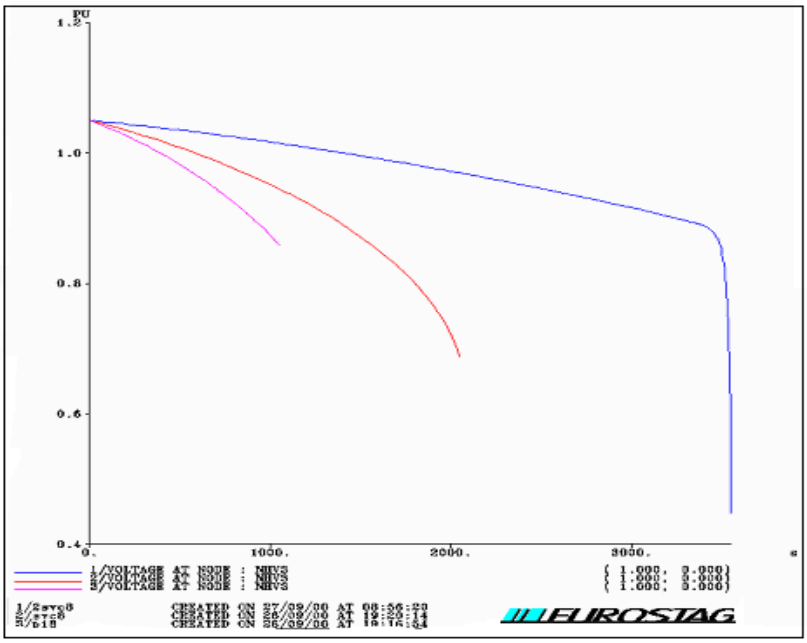

Figure 1-6 Effect of number of SVC on voltage stability. Top curve is when there are two SVC's and the middle curve is when there is one SVC at the middle of the line. For the bottom curve, there is no SVC.

It is seen that placement of a SVC affects the voltage collapse point. This can be seen in the Figure 1-7. The rightmost curve corresponds to placing a single SVC closer towards the load end. The middle curve corresponds to placing the SVC in the middle while the leftmost curve corresponds to placing the SVC towards the generating end.

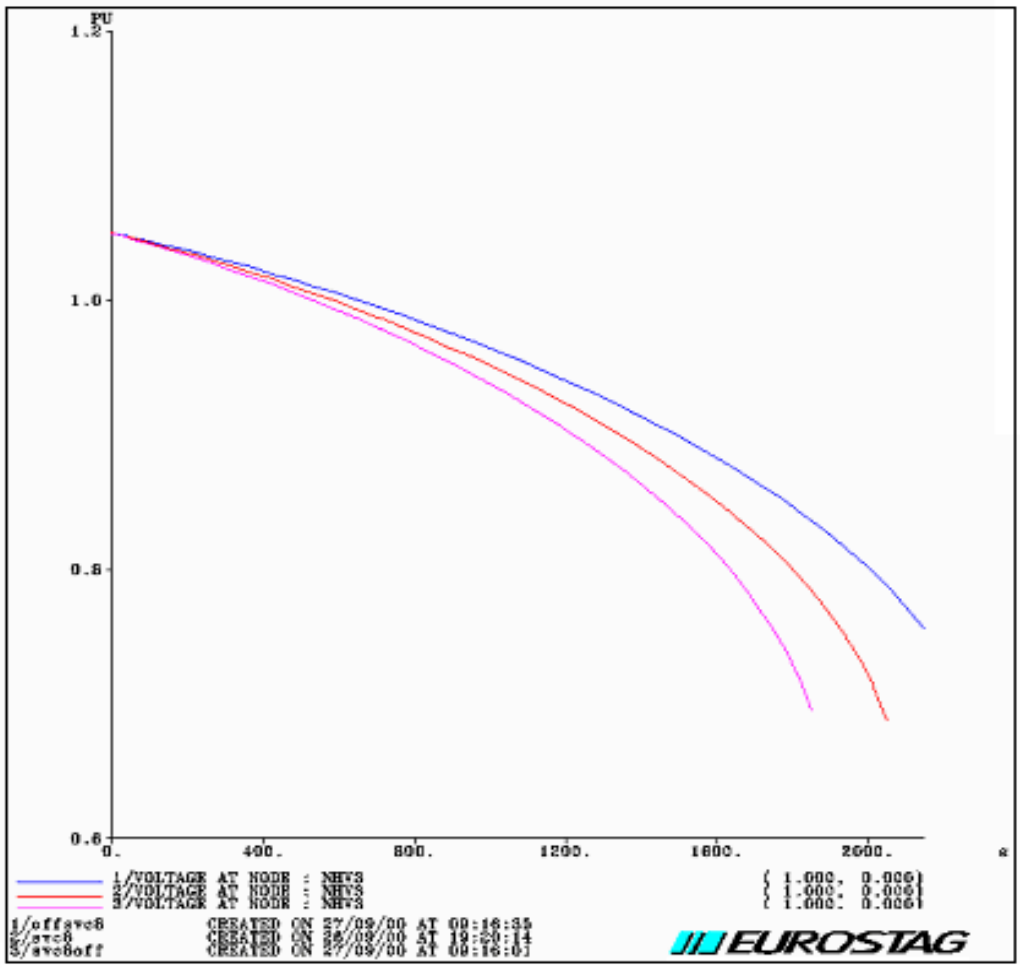

Figure 1-7 Effect of placement of SVC on voltage stability. Leftmost curve is when the SVC is close to generator end. The center curve gives the voltage profile when one SVC is at the middle of the line. The rightmost curve is when a SVC is close to load end.

1.5 Modeling of load and its effect on voltage stability margins

The load modeling equation has been taken from the textbook by Carson Taylor on voltage stability [13], and is given by the following expression:

$$P = P_0\left(\frac{U}{U_0}\right)^{Pv}\left(\frac{\omega}{\omega_0}\right)^{Pf}$$

$$Q = q_0\left(\frac{U}{U_0}\right)^{Qv}\left(\frac{\omega}{\omega_0}\right)^{Qf}$$

We have chosen three types of load where the coefficients are given as follows:

Lighting: Pv = 1.54, Pf = 0.0, Qv = Qf = 0.0, P.F. = 1.0

Central A/C: Pv = 0.2, P f= 0.9, Qv = 2.2, Qf = -2.7, P.F. = 0.81

Refrigerator: Pv = 0.8, Pf = 0.5, Qv = 2.5, Qf = -1.4, P.F. = 0.84

To get the following curves, the load was increased in all the three cases starting from 1MW. The voltage profile with respect to increased loading is shown in Figure 1-8.

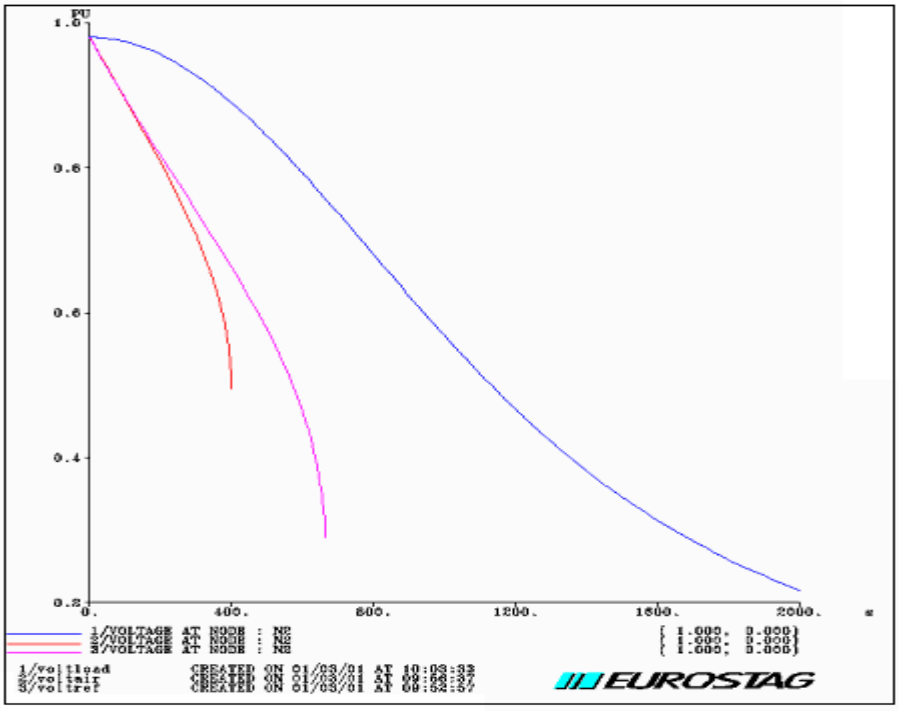

Figure 1-8 Effect of load type on voltage stability. Leftmost curve is for central A/C, middle curve for refrigeration, and rightmost curve for incandescent lighting.

It can be seen from the above figure that the A/C load becomes unstable at a higher voltage magnitude compared to the refrigerator and lighting load model cases. Thus, from viewpoint of severity of the load on voltage stability, the A/C load is the most severe, followed by the refrigerator load and finally the lighting load.

In case of the lighting load, it is seen to be stable at very low voltages. This can be explained by using Figure 1-9. The higher trace shows the power variations with time while the lower trace shows the voltage profile over time for the lighting load case.

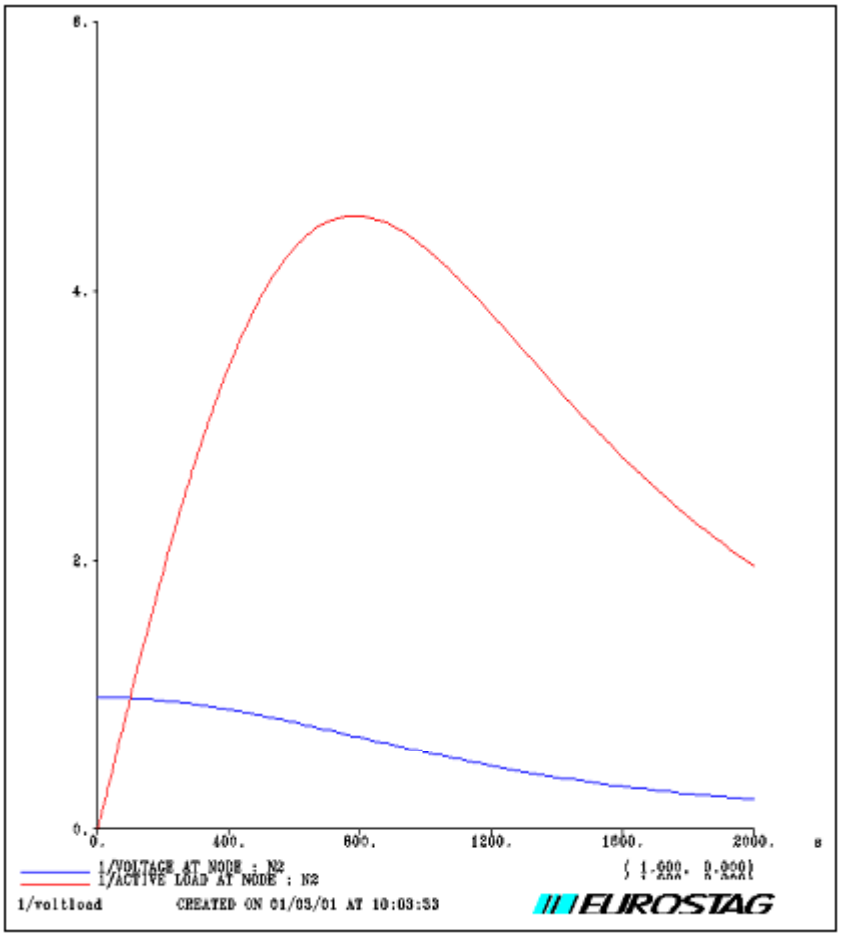

Figure 1-9 Power and voltage profile with increasing lighting load

It can be seen that, initially, power increases to a peak with a corresponding decrease in voltage. However, after peak is reached, the power decreases indicating stable operation at a low voltage solution usually represented in the lower half of the conventional PV curve representation.

1.6 Summary of observations for the two-bus case study

After running the simulations and observing the voltage collapse profiles, the following points became evident to us.

1) As X increases (longer lines), the collapse point lowers. This implies that the likelihood of voltage collapse is more in the case of loads supplied from generation over a long distance.

2) Lower power factor impedance loads causes voltage collapse at lower power levels. Hence, the limit of voltage stability margin for load buses operating at low power factors is less than load buses operating at high power factors.

3) It is very clearly seen from our simulations that the use of SVC's improves stability margin (i.e., the loading at which collapse point occurs). However, it is also seen that employing SVC's very near to the load improves voltage stability margin more than when it is employed farther from the load bus.

4) The effect of load type on voltage stability was brought out distinctly in our simulations. It can be seen from the simulation that voltage and frequency dependent loads (such as air conditioners and refrigerators) affect voltage collapse significantly.

2
Stability Index for Static Voltage Security Analysis

2.1 Voltage collapse point at load bus using a two-bus model

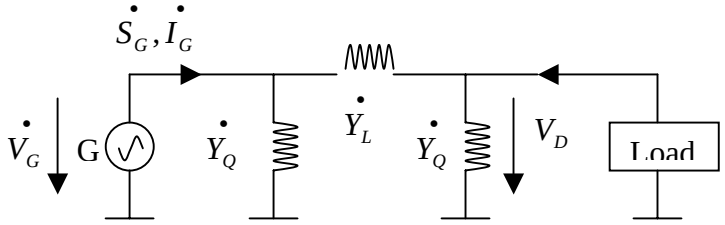

Figure 2-1 Single generator and single load system

The simple system in Figure 2-1 has a load bus and a generator bus. We are interested in their voltage behavior.

Using the nomenclature that a dot(.) on top of a variable indicates that it is a vector and a star(*) indicates it is the conjugate of that vector, we have:

$$\dot{I}_D = \dot{V}_D \dot{Y}_Q + (\dot{V}_D - \dot{V}_G)\dot{Y}_L = \frac{\overset{*}{S}_D}{\overset{*}{V}_D} \tag{2.1}$$

$$\overset{*}{S}_D = V_D{}^2 \dot{Y}_Q + V_D{}^2 \dot{Y}_L - \overset{*}{V}_D \dot{V}_G \dot{Y}_L = V_D{}^2 \dot{Y}_{11} + \dot{V}_0 \overset{*}{V}_D \dot{Y}_{11} \tag{2.2}$$

$$\text{Here } \dot{Y}_{11} = \dot{Y}_Q + \dot{Y}_L \text{ and } \dot{V}_0 = -\frac{\dot{Y}_L}{\dot{Y}_L + \dot{Y}_Q}\dot{V}_G \tag{2.3}$$

Since we would like to find the effect of load on the voltage, we would like to find solution of $\left|\dot{V}_D\right|$. We represent the magnitude of $\dot{V}_D$ as V_D in the equation (2.2).

Let $\frac{\overset{*}{S}_D}{\dot{Y}_{11}} = a + jb$. Then, equation (2.2) is expressed as follows:

$$\frac{\overset{*}{S}_D}{\dot{Y}_{11}} = a + jb = V_D{}^2 + \dot{V}_0 \overset{*}{V}_D = V_D{}^2 + V_0 V_D \cos(\delta_0 - \delta_D) + jV_0 V_D \sin(\delta_0 - \delta_D) \tag{2.4}$$

$$\cos\delta = \cos(\delta_0 - \delta_D) = \frac{a - {V_D}^2}{V_0 V_D} \tag{2.5}$$

$$\sin\delta = \sin(\delta_0 - \delta_D) = \frac{b}{V_0 V_D} \tag{2.6}$$

Summing up, after squaring equations (2.5) and (2.6), would lead to the following.

$${V_0}^2 {V_D}^2 = (a - {V_D}^2)^2 + b^2 = a^2 - 2a{V_D}^2 + {V_D}^4 + b^2 \tag{2.7}$$

Solving the equation (2.7) we get the following:

$$V_D = \sqrt{\frac{{V_0}^2}{2} + a \pm \sqrt{\frac{{V_0}^4}{4} + a{V_0}^2 - b^2}} = \sqrt{\frac{S_D}{Y_{11}}(r \pm \sqrt{r^2 - 1})} \tag{2.8}$$

because $\frac{\overset{*}{S}_D}{\dot{Y}_{11}} = a + jb$, hence $a = \frac{S_D}{Y_{11}}\cos(\phi_{S_D} + \phi_{Y_{11}})$, $b = -\frac{S_D}{Y_{11}}\sin(\phi_{S_D} + \phi_{Y_{11}})$. Then

$$V_D = \sqrt{\frac{{V_0}^2}{2} + a \pm \sqrt{(\frac{{V_0}^2}{2} + a)^2 - (a^2 + b^2)}}$$

$$= \sqrt{\frac{{V_0}^2}{2} + \frac{S_D}{Y_{11}}\cos(\phi_{S_D} + \phi_{Y_{11}}) \pm \sqrt{\left(\frac{{V_0}^2}{2} + \frac{S_D}{Y_{11}}\cos(\phi_{S_D} + \phi_{Y_{11}})\right)^2 - \frac{{S^2}_D}{{Y^2}_{11}}}}$$

$$= \sqrt{\frac{S_D}{Y_{11}}(r \pm \sqrt{r^2 - 1})} \tag{2.9}$$

Here r is defined as $r = \frac{{V_0}^2 Y_{11}}{2S_D} + \cos(\phi_{S_D} + \phi_{Y_{11}})$ (2.10)

2.1.1 Formulate a stability indicator

We can see that when $\sqrt{\frac{{V_0}^4}{4} + a{V_0}^2 - b^2} = 0$, the voltage at the node bus will collapse.

Now for $\dot{V}_0 = -\frac{\dot{Y}_L}{\dot{Y}_L + \dot{Y}_Q}\dot{V}_G$;

when $\frac{V_0^4}{4} + aV_0^2 - b^2 \geq 0$, the voltage at node bus will be sustained; when $\frac{V_0^4}{4} + aV_0^2 - b^2 < 0$, the voltage cannot be sustained.

That is to say, the voltage collapse threshold is expressed $a = \frac{b^2}{V_0^2} - \frac{V_0^2}{4}$.

Since $\frac{\overset{*}{S}_D}{\dot{Y}_{11}} = a + jb$, we can deduce the active power P_D and reactive power Q_D of $\dot{S}_D$ (where $\dot{S}_D = P_D + jQ_D$) as follows:

$$P_D = \mathrm{Re}(\dot{Y}_{11}(a + jb)), Q_D = \mathrm{Im}(\dot{Y}_{11}(a + jb))$$

We can get the corresponding curve in $\dot{S}_D$ complex plane.

Now, we can take this curve as the boundary of voltage collapse at the load node. This will help us formulate an indicator to reflect the proximity to this borderline. [14]

From equation (2.9), the voltage collapses when $r = 1, \frac{S_1}{V_D^2 Y_{11}} = 1$.

From the equation of (2.2), we can get:

$$\frac{\overset{*}{S}_1}{V_D^2 \dot{Y}_{11}} = 1 + \frac{\dot{V}_0}{\dot{V}_D} \tag{2.11}$$

So, we define an indicator L for voltage collapse as:

$$L \overset{\Delta}{=} \left| 1 + \frac{\dot{V}_0}{\dot{V}_D} \right| = \left| \frac{\overset{*}{S}_1}{V_D^2 \dot{Y}_{11}} \right| = \frac{S_1}{V_D^2 Y_{11}} \tag{2.12}$$

When the load is zero ($\dot{S}_1 = 0$), then L=0; if the voltage at bus 1 collapses, L=1.

Let us consider this problem from the viewpoint of Jacobian matrix singularity. If the voltage at the load bus collapses, then the Jacobian matrix will be singular; that is, the determinant of the matrix will equal to zero.

From equation (2.5) and (2.6), we can list the power flow equations for the above two-bus system as shown below:

$$f(V_D, \delta) = V_0 V_D \cos\delta + V_D^2 = a$$

$$g(V_D, \delta) = V_0 V_D \sin\delta = b$$

So, the corresponding Jacobian matrix is as follows:

$$J = \begin{bmatrix} 2V_D + V_0\cos\delta & -V_D V_0 \sin\delta \\ V_0 \sin\delta & V_D V_0 \cos\delta \end{bmatrix} \tag{2.13}$$

When the determinant of matrix J equals to zero, the voltage at the load bus will collapse:

$$\det(J) = 2{V_D}^2 V_0 \cos\delta + V_D {V_0}^2 = 0 \Rightarrow \frac{V_D \cos\delta}{V_0} = \mathrm{Re}\left\{\frac{\dot{V}_D}{\dot{V}_0}\right\} = -\frac{1}{2}$$

Then we can represent $\frac{\dot{V}_D}{\dot{V}_0} = -\frac{1}{2} + jb$ where b is a real number, leading to:

$$\left|1 + \frac{\dot{V}_0}{\dot{V}_D}\right| = \left|1 + \frac{1}{-\frac{1}{2} + jb}\right| = \left|\frac{\frac{1}{2} + jb}{-\frac{1}{2} + jb}\right| = 1 \tag{2.14}$$

Actually, when we divide equation (2.2) by ${V_D}^2 \dot{Y}_{11}$, we get:

$$\frac{\overset{*}{S}_1}{{V_D}^2 \dot{Y}_{11}} = 1 + \frac{\dot{V}_0}{\dot{V}_D} \tag{2.15}$$

From the above analysis, we confirm that the indicator of voltage stability at load bus is given by equation (2.12).

2.1.2 Numerical verification

A two-bus based simulation is used to illustrate how L indicates the voltage stability margin with a change in loading. The results of the simulation are shown in Figure 2-2.

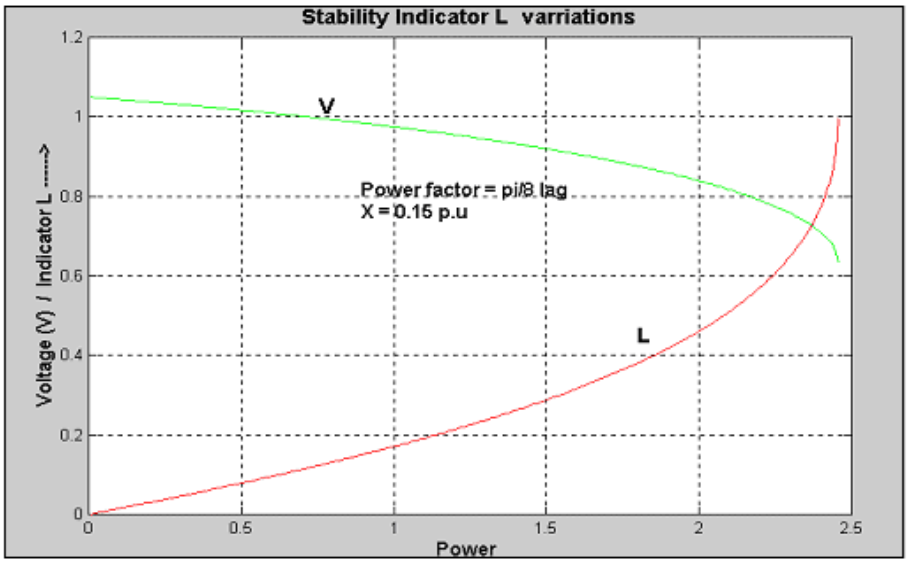

Figure 2-2 Voltage and indicator L with increased loading

2.1.3 Index L with TCSC for scenario given in section 1.3

In this case we will study how the indicator L behaves when we use a TCSC in the transmission line of a typical two-bus system. This is the same system as we used in section 1.3. The variation of indicator L with the change in transmission reactance, because of the TCSC impedance, is shown in the Figure 2-3.

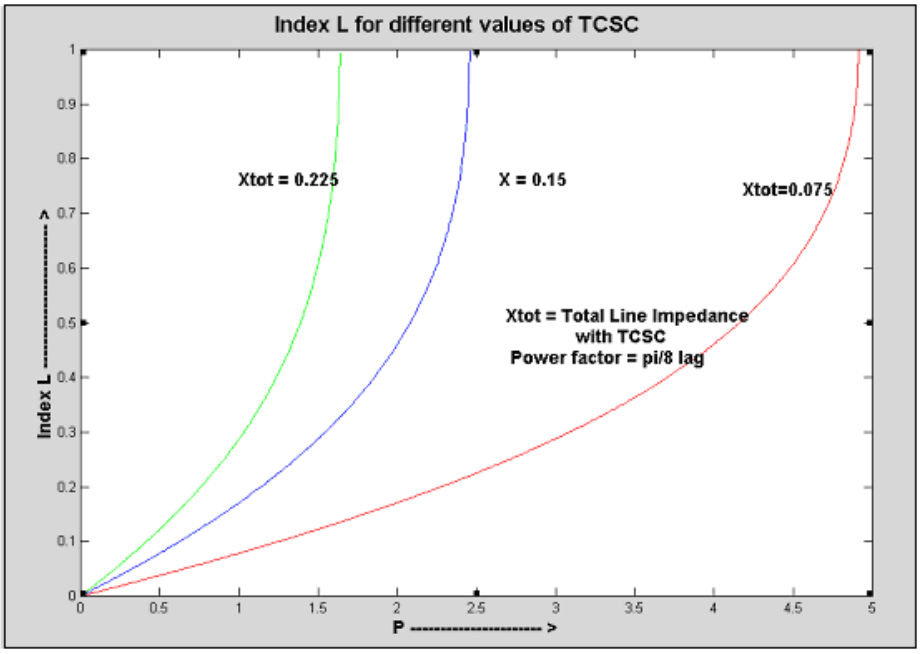

Figure 2-3 Effect of TCSC on index L

2.2 Extension of the two-bus voltage stability index L theory to a multi-bus system

We use the V and I to express the circuit of a n node system.

$$\begin{bmatrix} V_L \\ I_G \end{bmatrix} = H \begin{bmatrix} I_L \\ V_G \end{bmatrix} = \begin{bmatrix} Z_{LL} & F_{LG} \\ K_{GL} & Y_{GG} \end{bmatrix} \begin{bmatrix} I_L \\ V_G \end{bmatrix}$$

Here L denotes load and G denotes generator.

When we consider the voltage at load node j, we know that,

$$\dot{V}_j = \sum_{i \in L} \dot{Z}_{ji} \dot{I}_i + \sum_{i \in G} \dot{F}_{ji} \dot{V}_i \tag{2.16}$$

Carrying out the following transformations:

$\dot{V}_j - \sum_{i \in G} \dot{F}_{ji} \dot{V}_i = \sum_{i \in L} \dot{Z}_{ji} \dot{I}_i$. Multiplying $\overset{*}{V}_j$ at the both sides of the equation.

$V_j^{\,2} + \dot{V}_{0j} \overset{*}{V}_j = \overset{*}{V}_j \sum_{j \in L} \dot{Z}_{ji} \cdot \dot{I}_j$. Here $\dot{V}_{0j} = -\sum_{i \in G} \dot{F}_{ji} \dot{V}_i$.

$$= \overset{*}{V}_j (\dot{Z}_{jj} \cdot \dot{I}_j + (\sum_{\substack{i \in L \\ i \neq j}} \dot{Z}_{ji} \frac{\overset{*}{S}_i}{\overset{*}{V}_i}))$$

$$= \overset{*}{V}_j \cdot \dot{I}_j \cdot \dot{Z}_{jj} + \dot{Z}_{jj} (\sum_{\substack{i \in L \\ i \neq j}} \frac{\dot{Z}_{ji}}{\dot{Z}_{jj}} \frac{\overset{*}{S}_i}{\overset{*}{V}_i}) \overset{*}{V}_j$$

$= \overset{*}{S}_j \cdot \dot{Z}_{jj} + \dot{Z}_{jj} (\sum_{\substack{i \in L \\ i \neq j}} \frac{\dot{Z}_{ji}}{\dot{Z}_{jj}} \frac{\overset{*}{S}_i}{\overset{*}{V}_i}) \overset{*}{V}_j$. Let $\dot{Y}_{jj+} = \frac{1}{\dot{Z}_{jj}}$. Then,

$$= \frac{\overset{*}{S}_j}{\dot{Y}_{jj+}} + \frac{1}{\dot{Y}_{jj+}} (\sum_{\substack{i \in L \\ i \neq j}} \frac{\dot{Z}_{ji}}{\dot{Z}_{jj}} \frac{\overset{*}{S}_i}{\overset{*}{V}_i}) \overset{*}{V}_j$$

$= = \frac{\overset{*}{S}_j}{\dot{Y}_{jj+}} + \frac{\overset{*}{S}_{jcorr}}{\dot{Y}_{jj+}}$ in which $\dot{S}_{jcorr} = (\sum_{\substack{i \in L \\ i \neq j}} \frac{\overset{*}{Z}_{ji}}{\overset{*}{Z}_{jj}} \frac{\dot{S}_i}{\dot{V}_i}) \dot{V}_j$.

So, equation (2.16) can be transformed to:

$$V_j^{\,2} + \dot{V}_{0j}\overset{*}{V}_j = \frac{\overset{*}{S}_{j+}}{\dot{Y}_{jj+}} \tag{2.17}$$

and, as deduced from above,

$$\dot{V}_{0j} = -\sum_{i \in G} \dot{F}_{ji}\dot{V}_i$$

This can be regarded as an equivalent generator, including the contribution from all generators, such as the $\dot{V}_0$ for the two-bus case.

$$\dot{Y}_{jj+} = \frac{1}{\dot{Z}_{jj}}$$

$$\dot{S}_{j+} = \dot{S}_j + \dot{S}_{jcorr}$$

$\dot{S}_{jcorr} = (\sum_{\substack{i \in L \\ i \neq j}} \frac{\overset{*}{Z}_{ji}}{\overset{*}{Z}_{jj}} \frac{\dot{S}_i}{\dot{V}_i})\dot{V}_j$. This part expresses the contributions of the other loads at the node j.

This case can be considered equivalent to the single generator and single load system case. From the previous analysis, we know that:

$$L_j = \left| 1 + \frac{\dot{V}_{0j}}{\dot{V}_j} \right| = \left| \frac{\overset{*}{S}_{j+}}{\dot{Y}_{jj+} V_j^{\,2}} \right|$$

Thus, this gives an indicator of the proximity of a system to voltage collapse.

2.2.1 Multi-bus test system

The WSCC 9 bus system is taken as a sample system to illustrate the applicability of the indicator L to a multi-bus system. The test system is shown in Figure 2-4.

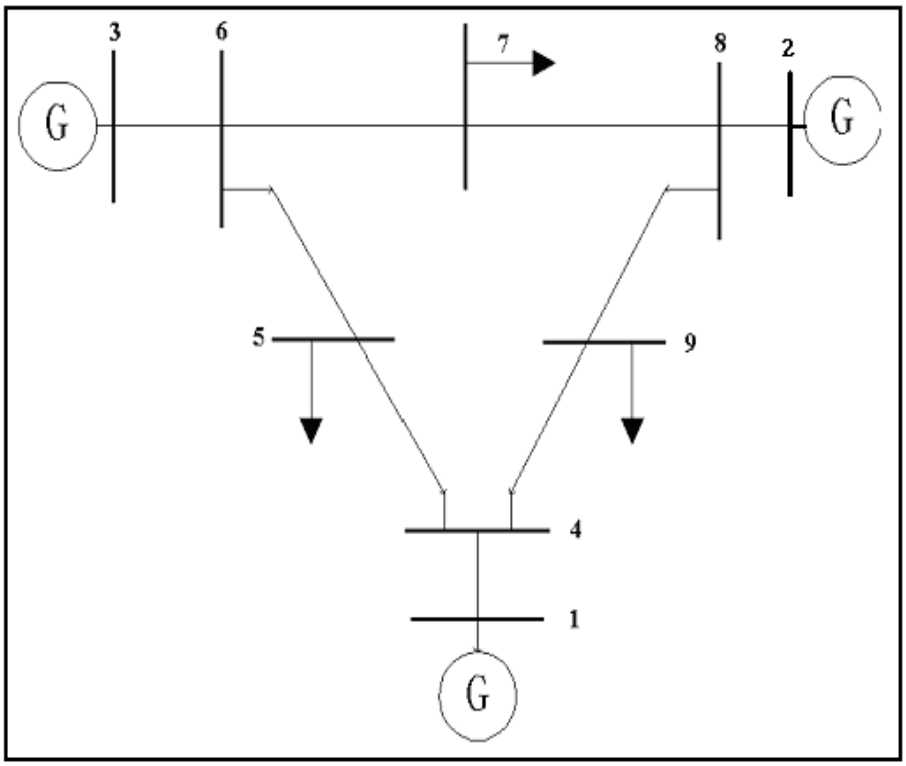

Figure 2-4 The WSCC 9 bus system

2.2.2 Case scenarios presented

The normal base loading at load buses are:

Bus 5: 90 + j 30 MVA
Bus 7: 100 + j 35 MVA
Bus 9: 125 + j 50 MVA

Buses 1 to 3 are generation buses; there are no generators or loads at buses 4, 6 and 8.

Three case scenarios have been simulated to study the steady state voltage collapse at the load buses and their respective L index.

Case I:

(a) Increase loading of bus 5 from zero to the voltage collapse point, keeping the load at other buses fixed at the normal value. Observe the effect on index L(5).
(b) Observe the effect on index L(7) at bus 7 when load at bus 5 is increasing and approaching collapse.

(c) Observe the effect on index L(6) at a bus 6, which is connected to bus 5 but has no load or generation.

Case II:

Increase loading of bus 7 from zero to the voltage collapse point keeping the load at other buses fixed at the normal value.

Case III:

Increase loading of bus 9 from zero to the voltage collapse point keeping the load at other buses fixed at the normal value.

(Note: Power factor is kept constant throughout the loading of buses.)

2.3 Results for the cases

The following sub-sections give the results obtained from the simulations.

2.3.1 Case I(a): Increasing load at bus 5 and observing the index L

As seen in Figure 2-5, index L approaches one at the collapse point. For this simulation, the load at bus 7 is taken as 100 + j 35 MVA and load at bus 9 is taken to be 125 + j50 MVA. The collapse occurs when the load at bus 5 is about 235 + j 217.11 MVA.

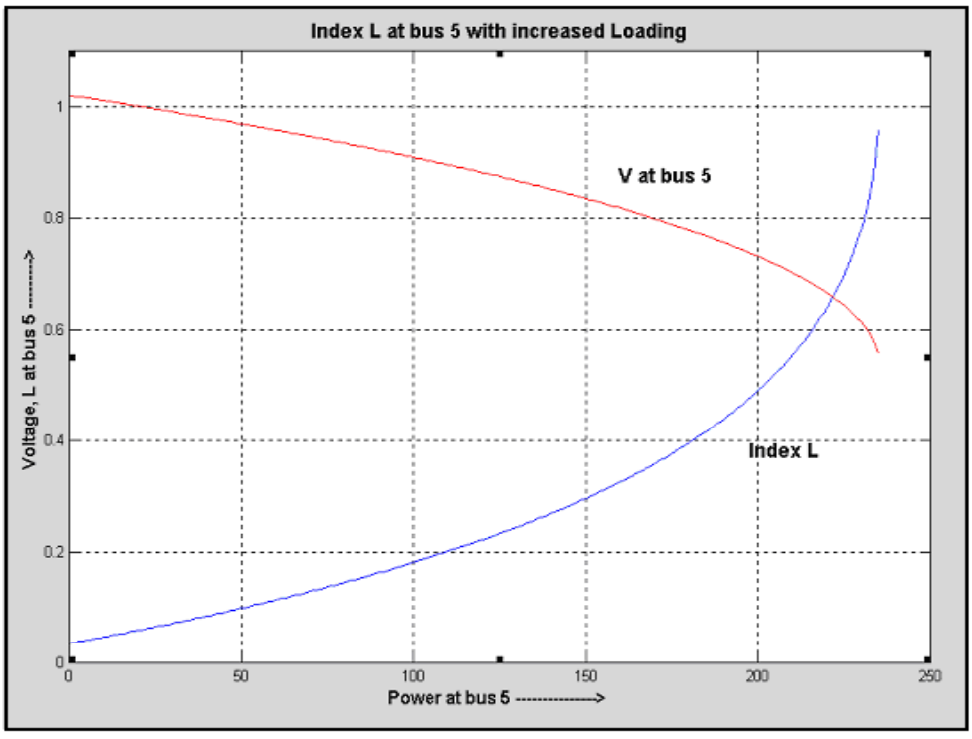

Figure 2-5 Index L at bus 5 with increased loading

2.3.2 Case I(b): Effect of index L, at distant load bus, with increased loading at local load bus

The index L at bus 7, L(7), is investigated for increasing load at bus 5. The load at bus 7 is fixed at 100+ j 35 MVA and bus 5 load is increased from 0 to the point of collapse that occurs at 235 + j217.11 MVA. It is found that L(7), in Figure 2-6, increases marginally from 0.0979 to 0.1990.

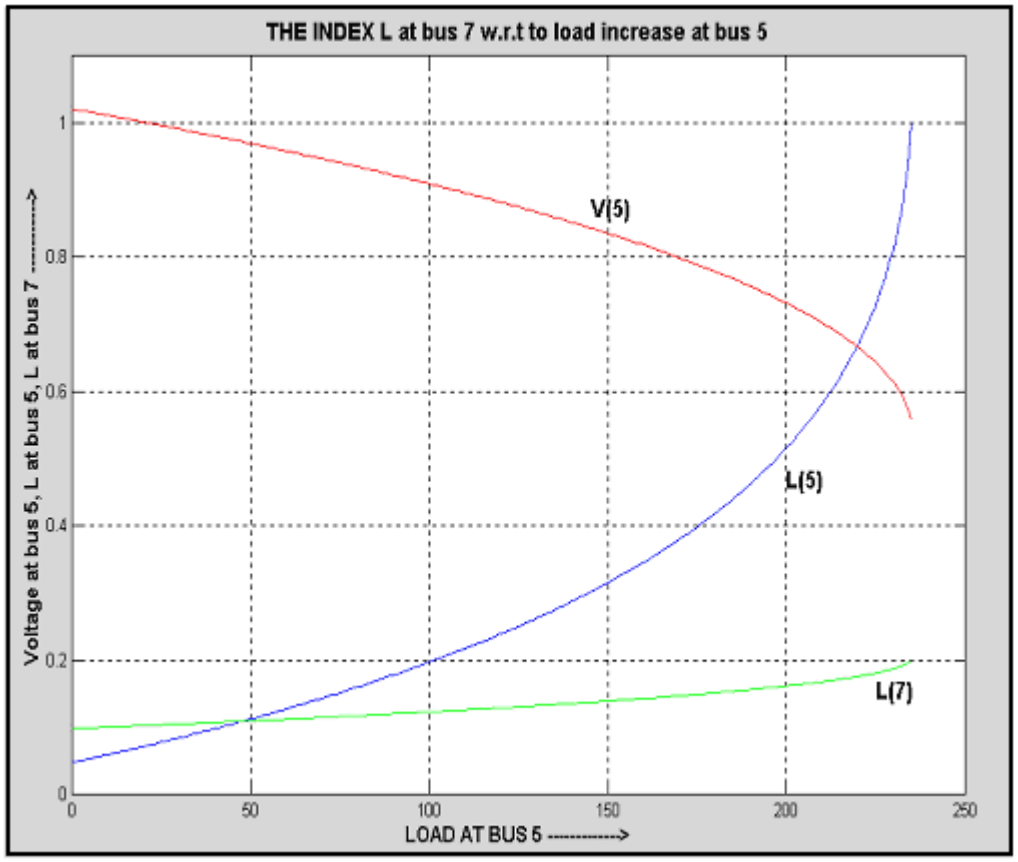

Figure 2-6 Index L for bus 7 with increased loading on bus 5

2.3.3 Case I(c): Effect of index L, at adjacent bus without load, with increased loading at local load bus

The index L at bus 6, L(6), is observed while increasing load at bus 5. There is no load at bus 6 and bus 5 load is increased from 0 to collapse that occurs at 235 + j 217.11 MVA. It is shown in Figure 2-7 that L(6) increases marginally from 0.0378 to 0.1682.

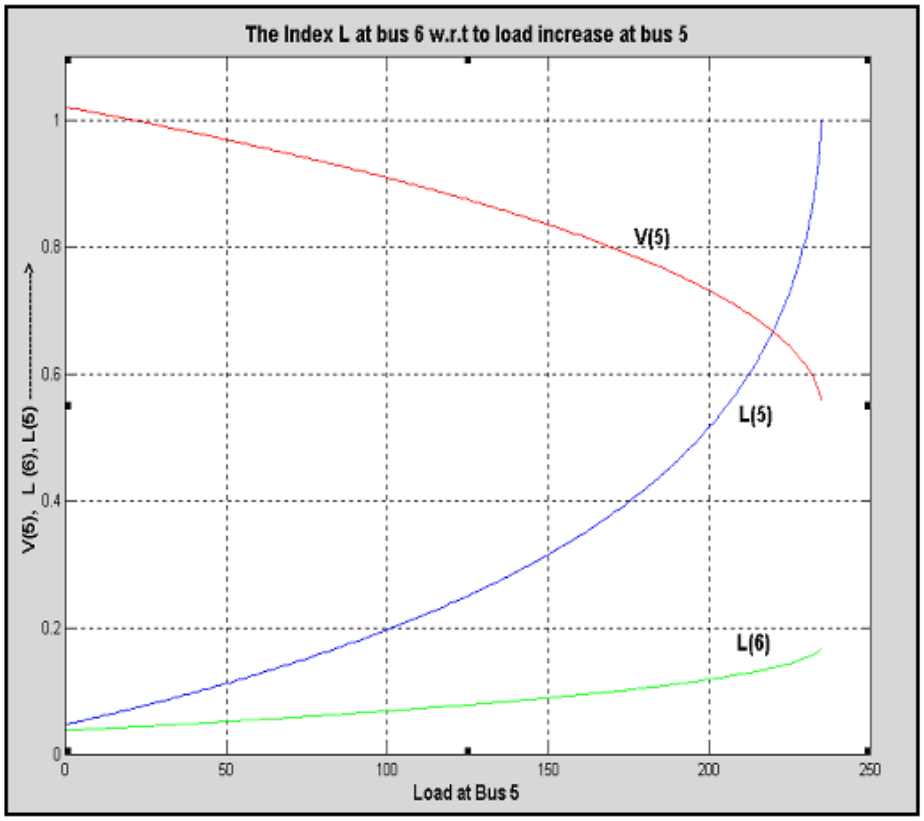

Figure 2-7 Index L for bus 6 with increased loading on bus 5

2.3.4 Case II: Increasing load at bus 7 and observing the index L

It is seen, in Figure 2-8 that index L approaches one at the collapse point. For this simulation, the load at bus 5 was 90 + j 30 MVA and load at bus 9 was 125 + j 50 MVA. The collapse occurs when the load at bus 7 is about 310.5+ j 286.86 MVA.

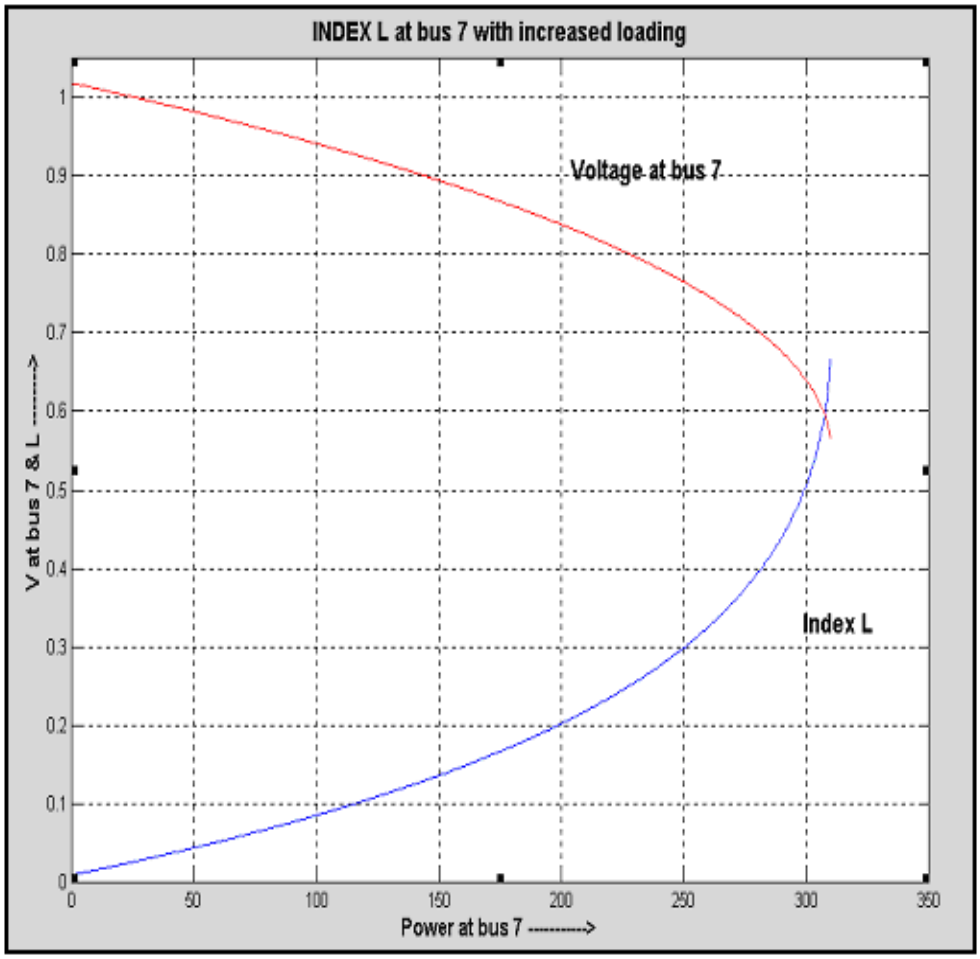

Figure 2-8 Index L at bus 7 with increased loading

2.3.5 Case III: Increasing load at bus 9 and observing the index L

As seen in Figure 2-9, the index L approaches one at the collapse point. For this simulation, the load at bus 5 was 90 + j 30 MVA and load at bus 7 was 100 + j 35 MVA. The collapse occurs when the load at bus 9 is about 251.5 + j 232.36 MVA.

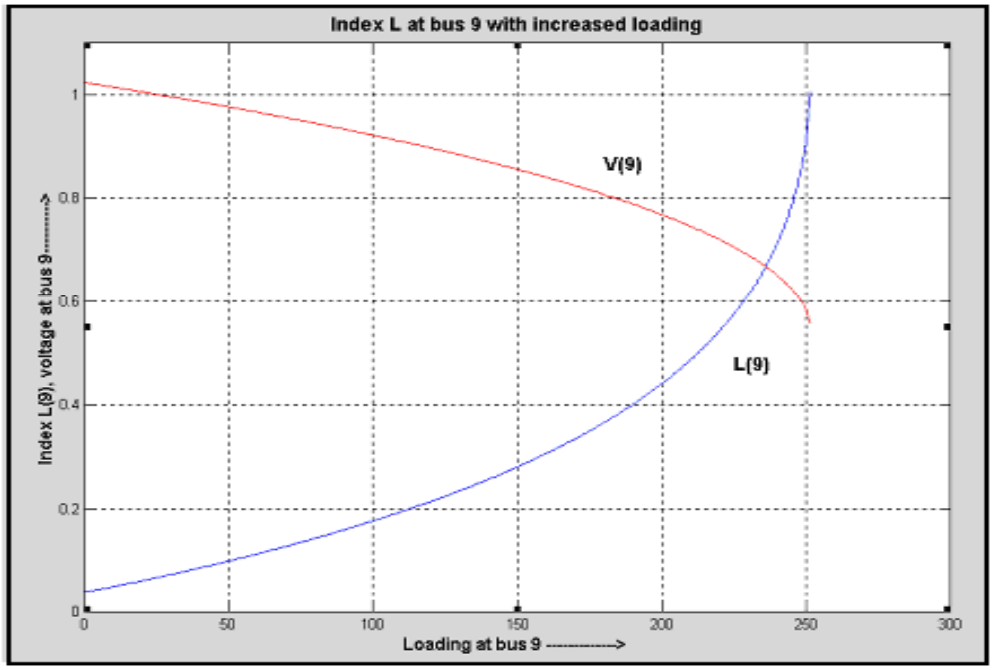

Figure 2-9 Index L at bus 9 with increased loading

2.3.6 Summary for the multi-bus scenarios

1) From the results of the simulations it can be distinctly observed that the index L for the bus in a multi-bus system approaches unity (1) at the steady state voltage collapse point.

2) The index L incorporates the effect of the load at the bus it is calculated, as well as the loading in the other parts of the system. However, the effect of other loads depends on how the bus under consideration is connected to the other buses.

3) There is no significant effect on the index value for a load bus that is not connected directly to the bus where voltage is collapsing.

4) For a bus (such as bus 6 which has no load and no generation) that is connected to a load bus (bus 5) on one end and a generator (bus 3) on the other end, the index (L(6) in this case) has only a marginal change as the load bus (bus 5) approaches collapse. This is because the voltage at that bus (bus 6) is being supported by the generator (at bus 3).

3
Dynamic Voltage Stability Issues

3.1 Applying index L to dynamic voltage stability studies

In this sub-section, whether the index L can be used as an early indicator of a dynamic voltage stability limit is investigated. The disturbances investigated are (1) a large step load change and (2) sudden loss of a transmission line.

The WSCC 9 bus system is used as a sample system to investigate the effects of dynamic voltage stability. This test system is the same one that was used in the previous chapter (shown in Figure 2-4)

.

The base case loadings for this simulation were:

Bus 5:	50 + j 40 MVA
Bus 7:	100 + j 35 MVA
Bus 9:	125 + j 50 MVA

The simulations have been done in EUROSTAG. Models for the exciter and governor have been included in all the generator models.

The L indices have been calculated on the same lines that discussed in the static voltage stability cases in the previous chapter. However, the voltages and the angles at the load buses are not the same during the dynamic time frame of interest. For simplicity, we have considered all the loads to be voltage and frequency independent.

Since the voltage at the generator buses is not held constant during the dynamic situation, the index L at each generator bus is evaluated considering other generator buses as constant PV buses. The method of calculation is similar to the one adopted for load buses.

The details of the analyses are given in the following sub-sections. In the simulations, only the governor and Automatic Voltage Regulator (AVR) have been modeled. Tap changers for transformers have not been incorporated.

3.2 Objective 1: Interaction of remote buses and local buses

We investigated the contributions of remote bus loads (bus 7 and bus 9) on index L at a local bus (bus 5) with respect to time. Table 3-1 shows the quantities used for computing the index for a step change of load at bus 5 from 50 + j 40 to 229.69 + j 183.7 MVA. This disturbance was initiated at the time of 10.0 seconds.

The index L is given by $L = | Sj^* / (Yjj+ x |V_5|^2) |$

where $Yjj+ = 1.6676 - j\ 11.3625$

and $Sj^* = \text{conj}(S_5 + S_7^* + S_9^*)$.

Here $S_5 = 2.2969 + j\ 1.837$

Time	S_7^*	S_9^*	$\lvert V_5 \rvert^2$	L
10.001	-0.1090 + j 0.0103	-0.2609 – j 0.0319	0.3588	0.7887
10.005	-0.1084 + j 0.0104	-0.2600 – j 0.0315	0.3552	0.7963
10.01	-0.1082 + j 0.0106	-0.2595 – j 0.0309	0.3528	0.8014
10.1	-0.1042 + j 0.0124	-0.2529 – j 0.0266	0.3226	0.8731
10.3	-0.0990 + j 0.0161	-0.2443 – j 0.0202	0.2884	0.9717
10.5	-0.1015 + j 0.017	-0.2499 – j 0.0215	0.3058	0.9182
15.0	-0.1116 + j 0.0139	-0.2670 – j 0.0324	0.3844	0.7374
50.0	-0.1113 + j 0.0147	-0.2670 – j 0.03241	0.3832	0.7396

Table 3-1 Evaluation of index L at bus 5

The following observations can be summarized based on the above simulation.

1) As can be seen from the values of the contributions for different buses, the variations in the real power component is not much. However, the reactive power component swings are perceptible. This is in line with the fact that voltage is related closely to reactive power.

2) The index L changes according to the local voltage profile and settles down to a definite value as the voltage settles down.

3.3 Objective 2: L as a dynamic stability indicator

We next assessed whether the index calculated at the first dip of the voltage at the bus where a step change in load has occurred can reveal information on dynamic stability.

This analysis was carried out because it was observed that the maximum value of L (when calculated over a time period) occurred at the first trough in the voltage profile. The disturbance is the same as discussed in objective 1.

The Table 3-2 has been tabulated for a range of step changes and gives the value of index L at the first big dip and the final settling value.

Power (MVA)	First Negative Peak L	Steady State L
50 + j 40	-	0.1135
200 + j 160	0.5224	0.4961
210 + j 168	0.5941	0.5548
220 + j 176	0.7002	0.6322
225 + j 180	0.7844	0.6818
229.6 + j 183.68	0.982	0.7396
229.65 + j 183.72	0.9963	0.7396
229.67 + j 183.736	1.0037	0.7396
229.68 + j 183.744	1.0109	0.7396

Table 3-2 Index L at the first big dip and the final settling value

The following observations can be made out based on this simulation.

1) Looking at the data of the power contributions from other load buses (buses 7 and 9 in our case) to the index calculated at the reference bus (bus 5 in our case), it is observed that the active component remains substantial even at higher loads compared with the initial value. However, considerable effect is reflected on the reactive power contributions. For example, at a load change from 50 + j 40 to 225 + j 180 at bus 5, the real part of S_9^* changed from 0.3421 to 0.2626. However, the reactive contribution dropped sharply from 0.1106 to 0.0367. This suggests two observations.

    a) The voltage at the bus nearing voltage collapse is strongly influenced by the reactive power demand at its bus.
    b) The effect of reactive power contributions of other load buses to the index is minimal. This supports our understanding that voltage collapse starts as a local phenomenon at a particular overloaded voltage bus (which is influenced strongly by its local reactive power requirement).

2) It is observed that the largest value of the index, which happens to occur at the first trough of the voltage after the load change, approaches one at the dynamic voltage collapse point. The final value of the index L matches with the value which was calculated for the steady state voltage stability case.

3.4 Objective 3: L as an overall system profile indicator

We next investigated the overall profile of the index variations at all load buses and all generator buses during a particular step load disturbance in one load bus.

A load change from 50 + j 40 to 229.6 + j 183.68 was imposed on load bus 5 at time = 10 seconds. The results for the evaluation of the indices as seen from the different buses are given below.

(a) Figure 3-1 shows the variations of all the indices with respect to time following the disturbance.

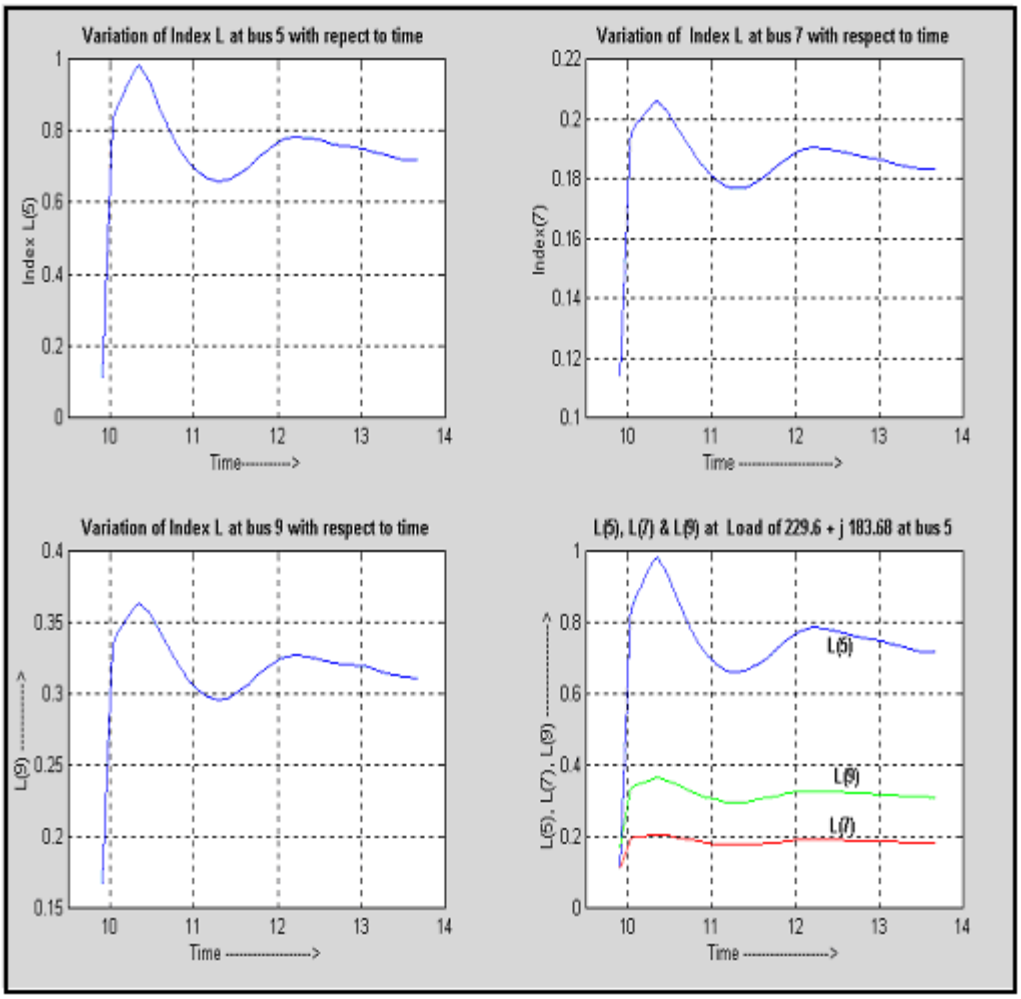

Figure 3-1 Variations of all the indices with respect to time

(b) Figure 3-2 includes the voltage and index variations for all load buses with respect to time, following the disturbance.

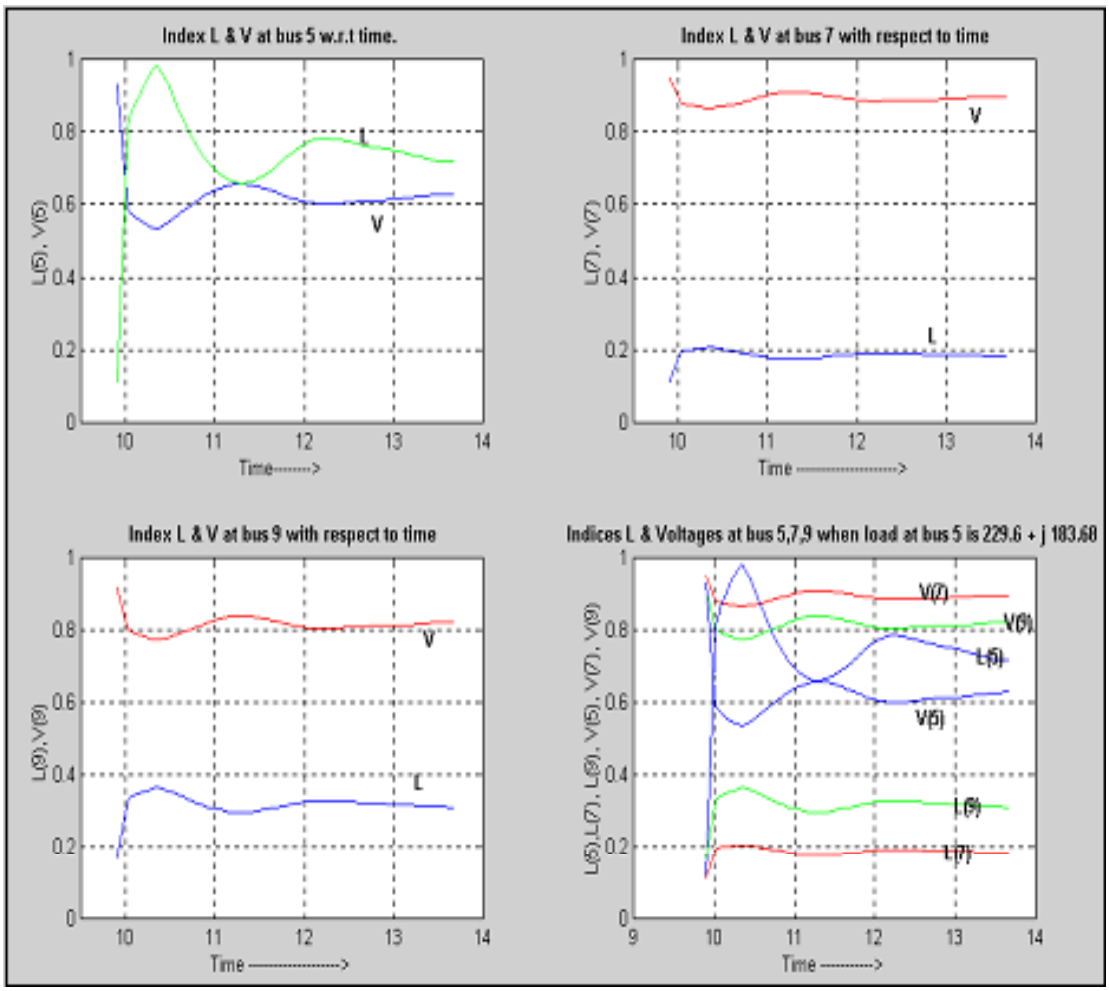

Figure 3-2 Voltage and index variations for all load buses

(c) Figure 3-3 shows the voltage and index variations at generator bus 1 with respect to time following the disturbance.

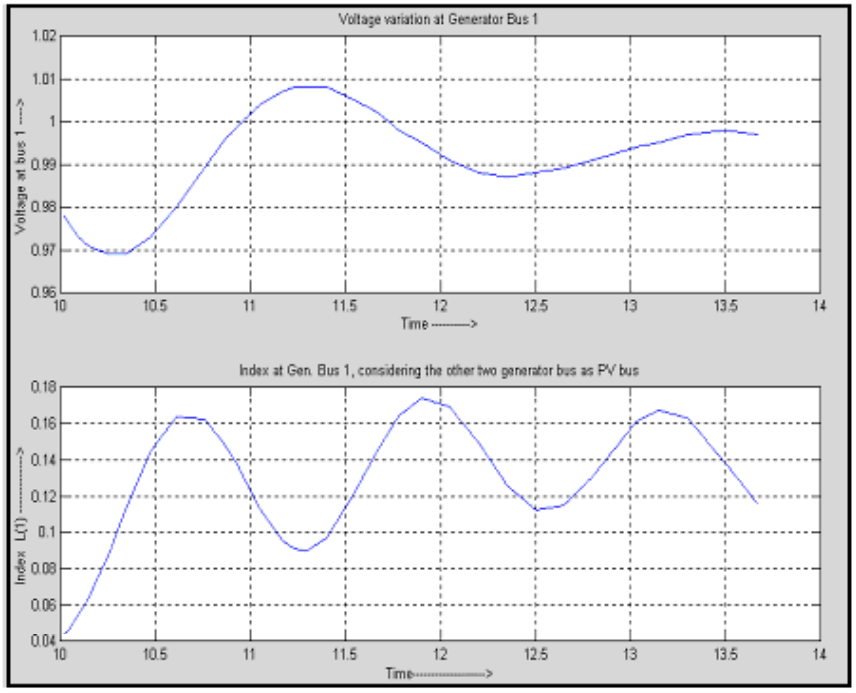

Figure 3-3 Voltage and index variations at generator bus 1

(d) Figure 3-4 shows the voltage and index variations at generator bus 2 with respect to time following the disturbance.

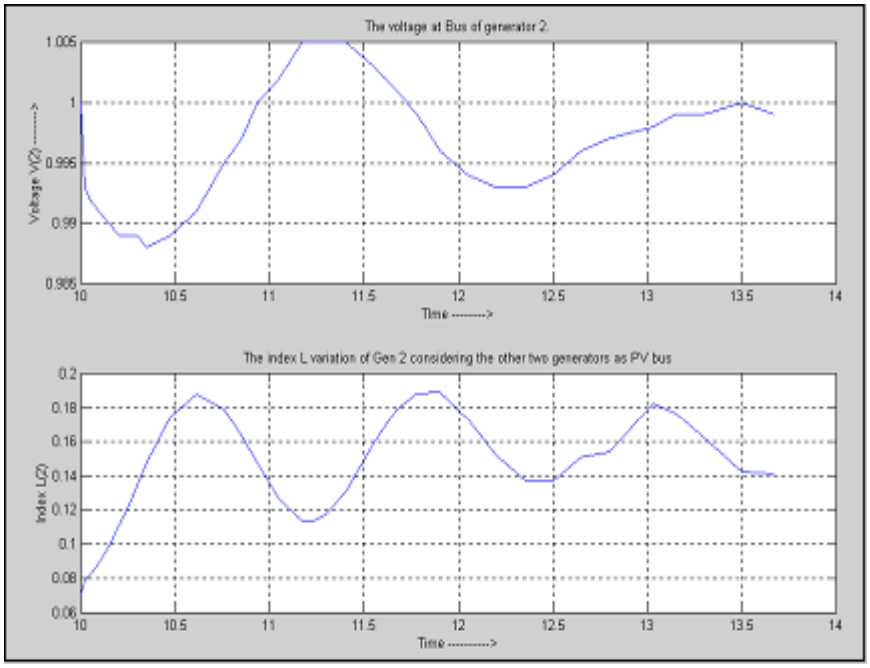

Figure 3-4 Voltage and index variations at generator bus 2

(e) Figure 3-5 shows the voltage and index variations at generator bus 3 with respect to time.

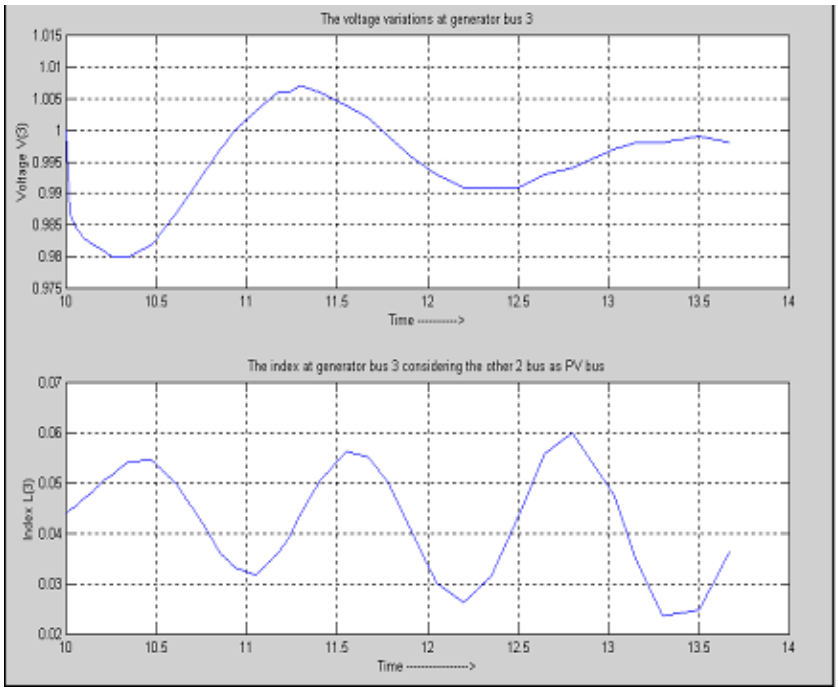

Figure 3-5 Voltage and index variations at generator bus 3

Based on the above simulations, the following observations can be made.

1) The index at generator bus 1 changes to a peak of around 0.1635 from an initial 0.0374. Looking at the position of bus 5 with respect to the generator bus 1, this seems reasonable. The load change affects the nearest generator the most. In this case, the line 4-5 impedance is less that line 5-6 impedance so load bus 5 is electrically closer to generator 1 than generator 3.

2) Near the dynamic collapse point, the increased loading at load bus 5 (to 229.6 + j 183.68) results in the index at load bus 9 rising from 0.1678 to 0.3166, thus decreasing its voltage stability margin. This might be due to the fact that generator 1, which has been affected by load bus 5 loading, is the nearest connected generator to load bus 9. (The impedance of line 4-9 is less than impedance 9-8.)

3) The index at load bus 7 changes from 0.1138 to around 0.1830 near the voltage collapse at load bus 5. The differential change in the index value is less than that in case of load bus 9. This might be explained by the fact that load bus 7 is supported by generator 3, which is affected the least by the disturbance. The L index calculated at generator bus 3 during the disturbance has peaked only to 0.0563 from an initial 0.0438.

3.5 Objective 4: L as stability indicator for loss of a line

We next observed whether the index calculated at the first dip of the voltage at the bus where a loss of line has occurred can reveal information of dynamic stability.

Figures 3-6, 3-7 and 3-8 shows the voltage profile at the load buses following the outage.

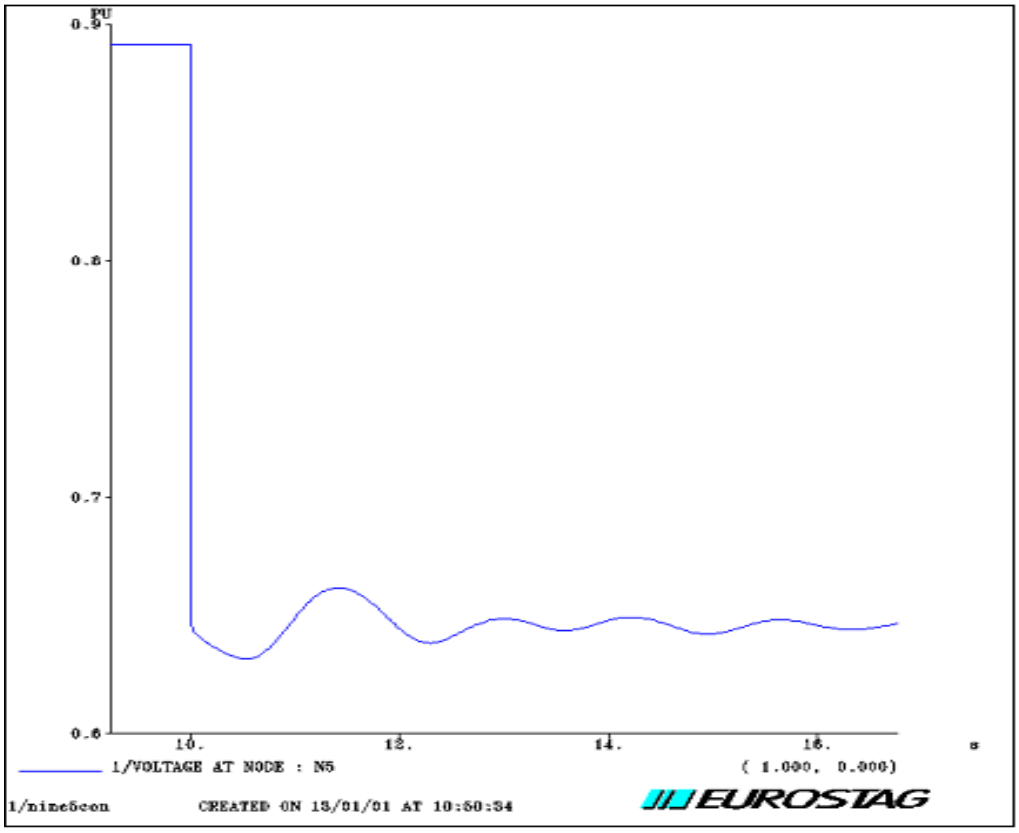

Figure 3-6 Voltage profile at bus 5 (having loading 90 + j 72) after loss of line 4-5

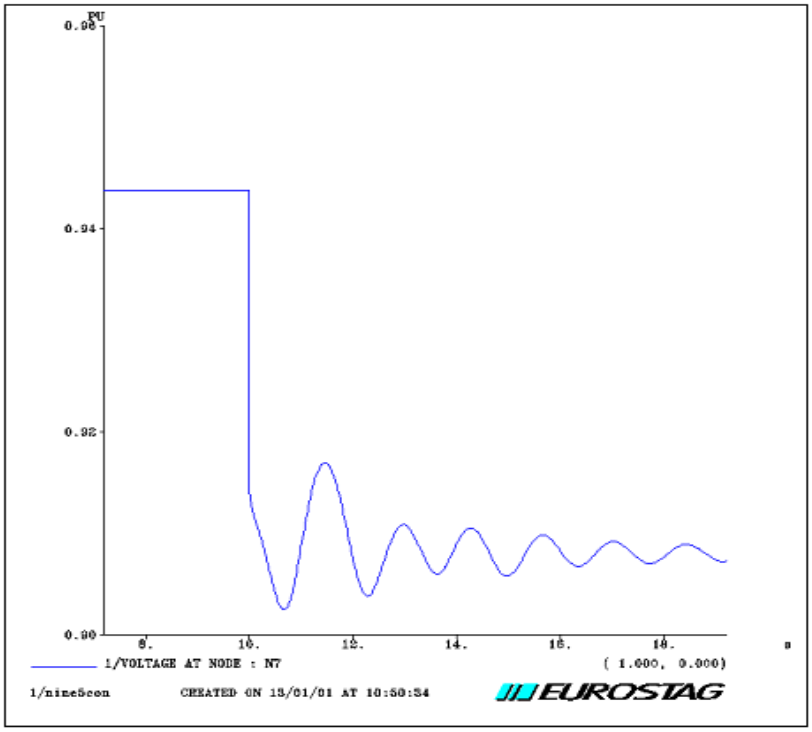

Figure 3-7 Voltage profile at bus 7 after loss of line 4-5

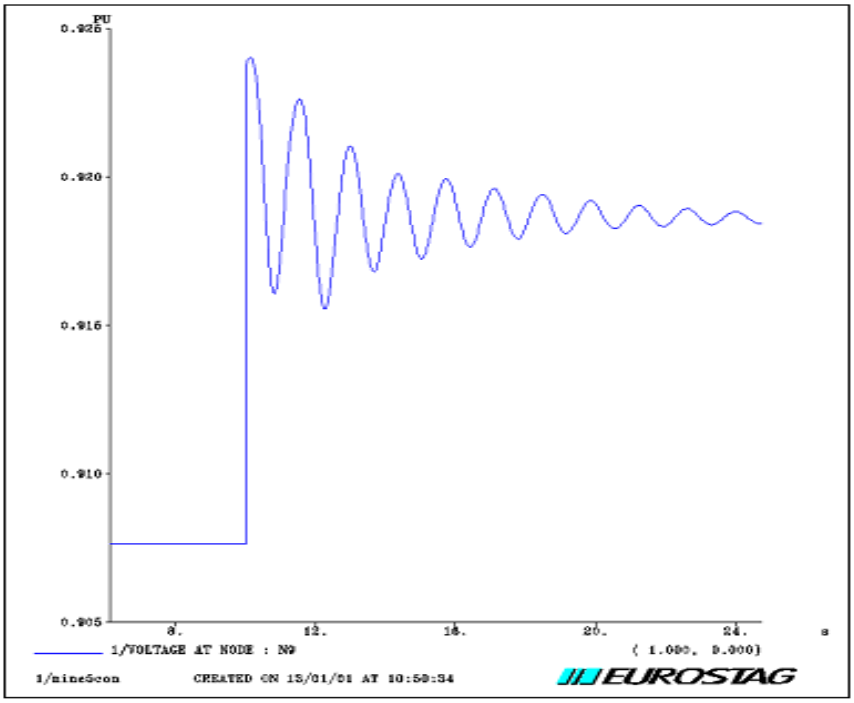

Figure 3-8 Voltage profile at bus 9 after loss of line 4-5

Tables 3-3, 3-4 and 3-5 show the index calculated (1) at the time of the largest dip (negative peak) in the voltage profile observed at bus 5, and (2) after the voltage oscillations dies down (i.e., steady state).

Power (MVA)	First Negative Peak L	Steady State L
50 + j 40	0.2312	0.2300
70 + j56	0.3706	0.3666
80 + j 64	0.4801	0.4722
90 + j 72	0.6787	0.6502
93 + j 74.4	0.8093	0.7508
93.5 + j 74.8	0.8645	0.7741
93.75 + j 75.0	0.8690	0.7860
93.9 + j 75.12	0.8850	0.7950
93.96 + j 75.168	0.8920	0.7980
93.97 + j 75.176	0.8951	0.7980

Table 3-3 Evaluation of index for bus 5 after loss of line 4-5

Power (MVA)	First Negative Peak L	Steady State L
50 + j 40	0.1241	0.1240
70 + j56	0.1370	0.1365
80 + j 64	0.1457	0.1448
90 + j 72	0.1584	0.1565
93 + j 74.4	0.1650	0.16194
93.5 + j 74.8	0.1670	0.1630
93.75 + j 75.0	0.1681	0.1634
93.9 + j 75.12	0.1689	0.164
93.96 + j 75.168	0.1690	0.1641
93.97 + j 75.176	0.1690	0.1641

Table 3-4 Evaluation of index for bus 7 after loss of line 4-5

Power (MVA)	First Negative Peak L	Steady State L
50 + j 40	0.1538	0.1541
70 + j56	0.1568	0.1573
80 + j 64	0.1592	0.1594
90 + j 72	0.16237	0.1627
93 + j 74.4	0.16399	0.16383
93.5 + j 74.8	0.16457	0.1640
93.75 + j 75.0	0.1647	0.1644
93.9 + j 75.12	0.1651	0.1645
93.96 + j 75.168	0.1652	0.1645
93.97 + j 75.176	0.1652	0.1645

Table 3-5 Evaluation of index for bus 9 after loss of line 4-5

3.5.1 Graphical plots for objective 4: L as stability indicator for loss of a line

(1) The Figure 3-9 shows the variations of the index at the load bus 5 with respect to its bus loading. Two curves are show: the peak index L (which occurs at the first largest negative dip in the voltage at bus 5 following the loss of line 4-5), and the index L evaluated after the voltage stabilizes down after the disturbance.

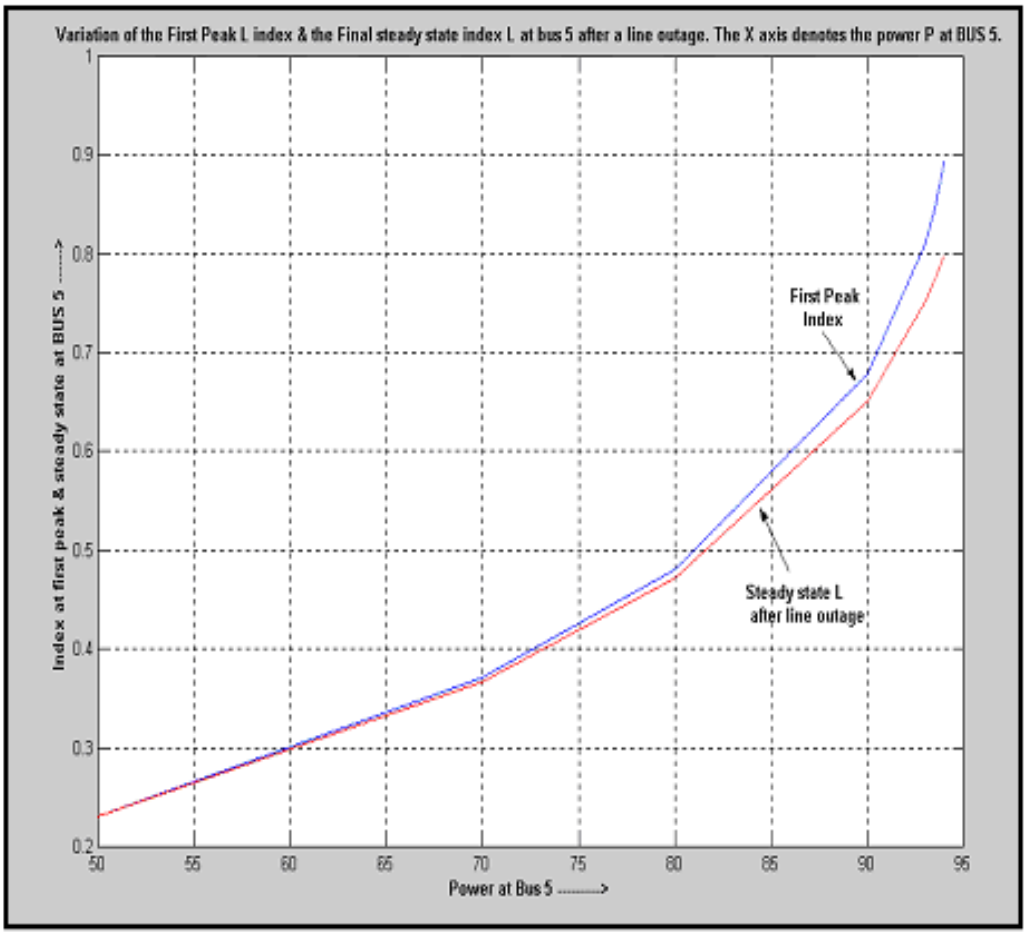

Figure 3-9 Variations of the index at load bus 5

(2) Figure 3-10 shows the variations of indices evaluated at bus 7 and bus 9 with respect to the loading at bus 5. The peak value (evaluated at the first largest negative dip in the voltage at bus 5 following the disturbance) and the steady state index value are plotted.

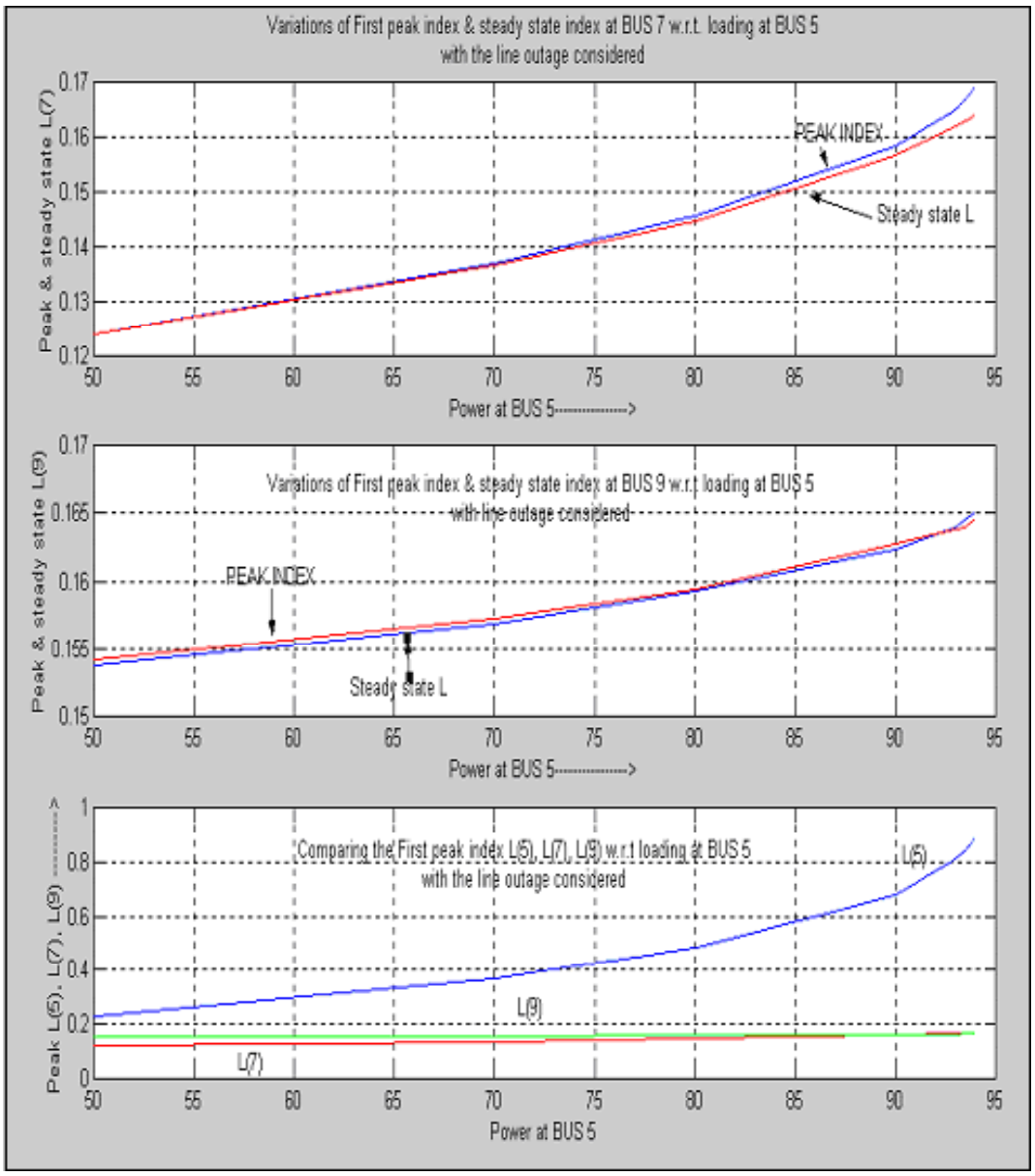

Figure 3-10 Variations of index evaluated at bus 7 and bus 9 with respect to the loading at bus 5

3.5.2 Observations for objective 4: L as stability indicator for loss of a line

1) The index, based on the information of the system at the first largest negative dip on bus 5, approaches one as the voltage collapse point nears.

2) The difference between the peak index and the steady state index does not vary much compared to the case of step load change, which was discussed in the earlier section.

3) The bus 5 collapsed around a load value of 94 + j75.2 dynamically because of line outage 4-5. The load at the steady state voltage stability limit evaluated for this case was 96.4 + j 89.06. Thus, the dynamic voltage stability limit calculated on the basis of a line outage is less than the steady state voltage stability limit.

4) The increase in index at buses 7 and 9 following loss of line 4-5 is marginal. This is because the line 4-5 outage does not directly influence these load centers. Moreover, since the real load at bus 5 is only about 0.9 p.u during its dynamic collapse, the impact of its transferred effect to load bus 7 and 9 is also minimal.

3.6 Objective 5: Impacts of Z on L as an indicator

We also investigated whether for the loss of line case for dynamic stability evaluation, the index calculated on the basis of exact local Z_{ii} term (considering the loss of line information), but with other impedance terms remaining the pre-contingency value, can still give a sufficiently accurate index calculation.

Tables 3-6, 3-7 and 3-8 give the result of calculating index considering the effect of the lost line 4-5 in calculating the Z_{LL} matrix, (stated as "Exact"), and taking only the Z_{ii} term taking the lost line 4-5 into consideration while the rest of the terms as the original healthy state Z_{LL} matrix. (stated as "Approximate").

Power (MVA)	Exact Peak Index	Approximate Peak L	Exact Steady Index	Approximate Steady L
50 + j 40	0.2312	0.2451	0.2300	0.2437
70 + j56	0.3706	0.3844	0.3666	0.3801
80 + j 64	0.4801	0.4938	0.4722	0.4855
90 + j 72	0.6787	0.6921	0.6502	0.6632
93 + j 74.4	0.8093	0.8228	0.7508	0.7636
93.5 + j 74.8	0.8645	0.8601	0.7741	0.7868
93.75 + j 75.0	0.8690	0.8826	0.7860	0.7988
93.9 + j 75.12	0.8850	0.8990	0.7950	0.8076
93.96 + j 75.168	0.8920	0.9056	0.7980	0.8107
93.97 + j 75.176	0.8951	0.9088	0.7980	0.8108

Table 3-6 Evaluation of index for bus 5

Power (MVA)	Exact Peak Index	Approximate Peak L	Exact Steady Index	Approximate Steady L
50 + j 40	0.1241	0.1174	0.1240	0.1174
70 + j56	0.1370	0.1254	0.1365	0.1251
80 + j 64	0.1457	0.1310	0.1448	0.1302
90 + j 72	0.1584	0.1389	0.1565	0.1376
93 + j 74.4	0.1650	0.1433	0.16194	0.1410
93.5 + j 74.8	0.1670	0.1445	0.1630	0.1417
93.75 + j 75.0	0.1681	0.1451	0.1634	0.1419
93.9 + j 75.12	0.1689	0.1456	0.164	0.1423
93.96 + j 75.168	0.1690	0.1457	0.1641	0.1423
93.97 + j 75.176	0.1690	0.1458	0.1641	0.1423

Table 3-7 Evaluation of index for bus 7

Power (MVA)	Exact Peak Index	Approximate Peak L	Exact Steady index	Approximate Steady (L)
50 + j 40	0.1538	0.1695	0.1541	0.1693
70 + j56	0.1568	0.1791	0.1573	0.1794
80 + j 64	0.1592	0.1855	0.1594	0.1853
90 + j 72	0.16237	0.1941	0.1627	0.1937
93 + j 74.4	0.16399	0.1986	0.16383	0.1970
93.5 + j 74.8	0.16457	0.1999	0.1640	0.1980
93.75 + j 75.0	0.1647	0.2004	0.1644	0.1983
93.9 + j 75.12	0.1651	0.2012	0.1645	0.1985
93.96 + j 75.168	0.1652	0.2013	0.1645	0.1986
93.97 + j 75.176	0.1652	0.2014	0.1645	0.1986

Table 3-8 Evaluation of index for bus 9

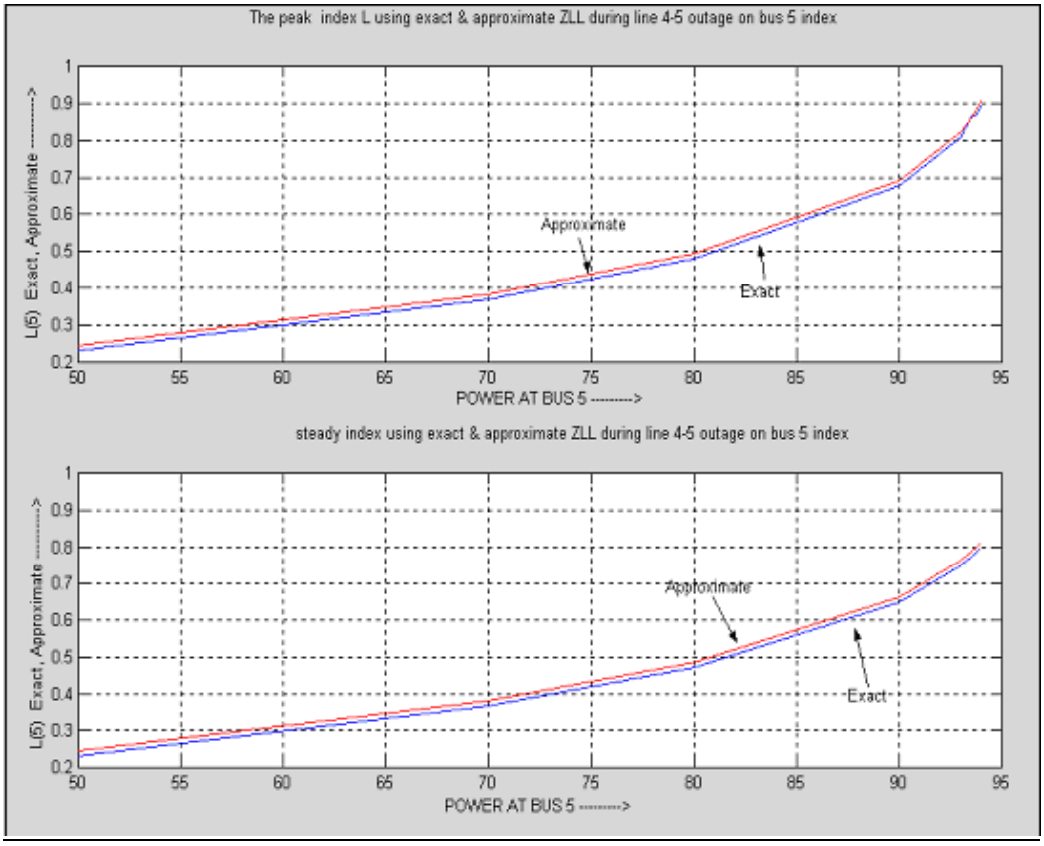

Figure 3-11 Index L value computed exactly and after approximation

The following observations can be made based on this simulation.

1) The Exact and the Approximate values match closely for all the load buses. Thus, the index is predominantly dependent on the term Z_{ii} of the Z_{LL} matrix.

2) If any local measurement at load buses can yield this value, then the index L calculated would be fairly approximate to the exact value, even if we cannot get the complete information of all the healthy lines in the network.

3.7 Publications

The readers can refer to reference [4] for summary of the work that has been discussed in the earlier sections of this chapter.

The dynamic modeling of generators, governors, ULTC, switched capacitor and loads using EUROSTAG have also been carried to study dynamic voltage stability [8]. The various myths surrounding dynamic voltage stability have been clarified here. Moreover, the importance of dynamic reserves of generation to maintain voltage stability during a dynamic disturbance has been clearly demonstrated in the simulations. Interested readers may refer to publication [8] for details about the simulation and the summary of the results.

4
Voltage Stability Constrained OPF Algorithm

As demonstrated in Chapter 3, the voltage stability index L represents, in a way, how far the load bus is from the voltage collapse point. This feature can be exploited in developing a load curtailment policy incorporating the security feature of voltage stability margin. The following section proposes a method to achieve this.

4.1 Algorithm

The following steps explain the procedure of carrying out an optimal power flow (OPF) with the index L_i at load buses as one of the constraints.

The **objective function** is minimization of load curtailed, or

$$minimize \sum_{i=1}^{n} Load - Curtailment_i$$

For all buses from i =1,2…n

For each bus i, the term Load-Curtailment$_i$ is given by the following expression:

$$Load - Curtailment_i = P_{lireq} - P_{li}$$

Here P_{lireq} is the load demand that is to be satisfied at bus i before the OPF procedure. P_{li} is the load demand that can actually be met, within the constraint specified, after the OPF.

For all the buses, the power flow equations to be satisfied are:

$$P_{gi} - P_{li} - \sum_{j=1}^{n} V_i V_j (G_{ij} \cos\delta_{ij} + B_{ij} \sin\delta_{ij}) = 0$$

$$Q_{gi} - Q_{li} - \sum_{j=1}^{n} V_i V_j (G_{ij} \sin\delta_{ij} - B_{ij} \cos\delta_{ij}) = 0$$

The minimum and maximum limits on generators active and reactive power output is given by:

$$P_{gi\,min} \le P_{gi} \le P_{gi\,max}$$

$$Q_{gi\,min} \le Q_{gi} \le Q_{gi\,max}$$

The transmission line constraints can be specified by,

$$P_{ij}^2 + Q_{ij}^2 \leq S_{ij\,max}^2$$

The load shedding philosophy can be simplified if we assume that shedding is carried out in equal proportion of active and reactive power. In other words, the power factor of all the loads remains the same as the initial value. This can be represented as:

$$P_{li} / P_{lireq} = Q_{li} / Q_{lireq}$$

$$0 \leq P_{li} \leq P_{lireq} \qquad 0 \leq Q_{li} \leq Q_{lireq}$$

The following constraints are added to the OPF formulation to incorporate voltage stability.

(a) For all buses i, include the following constraints, as usually found in OPF formulations.

$$V_{i\,min} \leq V_i \leq V_{i\,max}$$

(b) For all the load buses (PQ) and buses where there are no loads and generators i, use the following additional constraint, based on local index calculation L_i.

$$L_i \leq L_{crit}$$

4.2 An illustration

The WSCC 9 bus system is taken as a sample system to illustrate the applicability of the indicator L to a multi-bus system. The test system is the same one that was used in section 2.2.1.

The following loads are in the system:

Bus 5: 150 + j 120 MVA
Bus 7: 100 + j 35 MVA
Bus 9: 125 + j 50 MVA

Table 4-1 gives the result of the OPF run based on the proposed algorithm for the above case. There is no load curtailment on bus 7 and bus 9. Only bus 5 has load curtailment.

NOTE: All the PV buses are held at V = 1.0 p.u.

L_{crit} for all the load buses	Load curtailment at bus 5
0.1	90.57 + j 72.45
0.2	36.45 + j 291.6
0.25	26.51 + j 21.21

Table 4-1 Results after the OPF

Without the constraint of voltage stability index imposed on the load buses, the load curtailment value at bus 5 after running OPF was found to be 26.51 + j 21.21.

4.3 Observations

1) For the above case, if we choose any value of L_{crit} just above 0.21, the voltage stability index constraint does not seem to affect the OPF solution for our load pattern and system chosen. This is because the constraint V_{min} is already violated and, hence, is held constant at the violated bus. Thereafter, the algorithm stops searching for a solution based on the voltage stability index constraint criterion.

2) The choice of a low value of L_{crit} increases the required load curtailment. Therefore, the above OPF algorithm encompasses the security-based feature of voltage stability in the calculation of load curtailment.

3) If the allowable V_{min} for bus 5 were kept as 0.8 p.u., the load curtailment using the stability margin criterion for L_{crit} of 0.3 was found out to be more than that calculated without using it.

4.4 Publications

For interested readers, further simulation and application details of the algorithm can be obtained from reference [1].

The authors have also formulated the algorithm to incorporate FACTS devices such as TCSC, the detail of which can be obtained from reference [2]. The loadability of the system can be increased by using these devices. The voltage stability constrained OPF algorithm, developed in this project, blends itself effectively to the steady state characteristic of the devices within its formulation.

Application of the algorithm to composite reliability analysis has been explored in reference [3]. Evaluation of reliability indices that incorporates the steady state voltage stability could be achieved using the algorithm.

5
Transaction-Based Stability Margin and Utilization Factors Evaluation

5.1 Theory behind transaction-based power flow

To derive a more complete formula of decomposition, we begin with the coupled AC power flow equations in *polar form* as follows.

$$\begin{cases} (P_{Gi} - P_{Di}) - V_i \sum_{j \in i} (g_{ij} \cos\theta_{ij} + b_{ij} \sin\theta_{ij}) = 0 \\ (Q_{Gi} - Q_{Di}) - V_i \sum_{j \in i} (g_{ij} \sin\theta_{ij} - b_{ij} \cos\theta_{ij}) = 0 \end{cases} \tag{5.1}$$

For $i = 1,2...,n \quad (i \neq s)$ (s is the slack bus), P_{Gi}, Q_{Gi} are active and reactive power generations at bus i; P_{Di}, Q_{Di} are active and reactive power loads at bus i; $V_i \angle \theta_i$ is the voltage magnitude and angle of bus i; $\theta_{ij} = \theta_i - \theta_j$; $y_{ij} = g_{ij} + jb_{ij}$ is the branch admittance between nodes i and j.

Let (V, θ) be the solution of the power flow equations (5.1). Several basic facts with respect to a general transmission system are observed below.

(1) Line resistance is considered much smaller than line reactance (i.e., r/x <<1), and voltage angle differences across each branch are assumed to be small.

(2) Active power flows in the system are strongly coupled with voltage angle differences across branches.

(3) Reactive power flows in the system are strongly coupled with the voltage magnitudes *V* throughout the entire network.

(4) When the absolute value of voltage angle θ is small enough throughout the system, nodal imaginary current components are strongly coupled with the voltage magnitudes *V*.

Facts 1, 2 and 3 are widely recognized, and used in DC flow analysis and other linearized flow models. In general Fact 4 holds on the conditions $r/x \leq 1/3$ and $|\theta| \leq \pi/9$, which is rather straightforward from the nodal voltage and current equation.

Let Y_{bus} be the (n×n) nodal admittance matrix, and $Z_{bus} = [Y_{bus}]^{-1}$, we consider the following nodal voltage equation,

$$\left[Ve^{j\theta}\right] = \left[Z_{bus}\right] \times \left[I_R + jI_M\right], \text{where } I_R = \mathrm{Re}(I_{bus}), I_M = \mathrm{Im}(I_{bus})$$

Approximately, the equation is satisfied when $\begin{cases} V\cos\theta \approx j[Z_{bus}][I_M] \\ V\sin\theta \approx [Z_{bus}][I_R] \end{cases}$ for $\frac{r}{x} \le \frac{1}{3}$

Now for $\cos\theta \approx 1$ for $|\theta| \le \pi/9$, we derive $|Ve^{j\theta}| = |V\cos\theta + V\sin\theta| \approx V\cos\theta$. That is, $V \approx j[Z_{bus}][I_M]$.

In the case of a constant Z_{bus}, it follows that the voltage magnitudes V strongly couple with the imaginary current components I_M on the conditions that $r/x \le 1/3$ and $|\theta| \le \pi/9$.

These facts are used to exploit relations between a particular nodal real power P_i and associated nodal current I_i. From Kirchhoff Laws, a real power injection P_i can be expressed in terms of real and imaginary current components. That is,

$$P_i = \mathrm{Re}[V_i e^{j\theta_i} \times (I_i^*)] = V_i \cos\theta_i \,\mathrm{Re}(I_i) + V_i \sin\theta_i \,\mathrm{Im}(I_i) \qquad (5.2)$$

It seems impossible to separate particular contributions of P_i on real and imaginary current components from equation (5.2). Fortunately, the facts as mentioned above enable us to make appropriate approximations as follows.

(i) When the second term of equation (5.2), $V_i \sin\theta_i \,\mathrm{Im}(I_i)$, is small, P_i can be approximately related to the real current component $\mathrm{Re}(I_i)$ by:

$$\mathrm{Re}(I_i) \approx \frac{P_i}{V_i \cos\theta_i} \qquad (5.3)$$

(ii) The remaining terms including all $\mathrm{Im}(I_i)$ and residual errors associated with $\mathrm{Re}(I_i)$ are approximately attributed to the system reactive power flows, which dominate the network voltage profiles.

Thus, the current injection vector of the reactive power market is approximated by:

$$I^Q = I_{bus} - \sum \mathrm{Re}(I^k) \qquad (5.4)$$

The accuracy of equation (5.3) depends on $V_i \sin\theta_i \,\mathrm{Im}(I_i)$, which is the approximation error. A relative approximation error on a basis of P_i is introduced below.

$$E_{Pi} = V_i \sin\theta_i \,\mathrm{Im}(I_i) / P_i = -\frac{\sin\theta_i \sin(\varphi_i - \theta_i)}{\cos\varphi_i} \tag{5.5}$$

E_{Pi} depends on the phase angle θ_i and power factor (PF) angle φ_i. To secure dynamic reactive power reserves, the normal PF on the demand side is restricted to a narrow margin (say $\cos\varphi \geq 0.90$ in lagging).

Two approximation error levels are marked:

Level 1*:* $|E_{Pi}| \leq 0.065$*, for* $-6.5 \leq \theta_i \leq 15$ *deg.*

Level 2*:* $|E_{Pi}| \leq 0.115$*, for* $-10 \leq \theta_i \leq 20$ *deg.*

Given a range of $-10 \leq \theta \leq 20$ degrees, the largest approximation error is around 10 percent.

For example, from a standard power flow solution, a range of appropriate reference angles to reduce approximation errors can be determined by:

$$\theta_{L,\min} - \theta_{\min} \leq \theta_s \leq \theta_{L,\max} - \theta_{\max} \tag{5.6}$$

where $\theta_{\max}, \theta_{\min}$ are the largest and smallest phase angles corresponding to a zero reference angle; and $\theta_{L,\min}, \theta_{L,\max}$ are the lower and upper limits of Level 1 or 2.

5.2 Transaction-based power flow algorithm

5.2.1 Assumptions

To begin with the decomposition algorithm, we first introduce economic contexts and involved assumptions.

(1) An energy market consists of individual energy scheduling coordinators SC_k, who are entitled to arrange MW exchange schedules and to choose loss suppliers.

(2) A SC_k may not maintain its own reactive power balance. Instead, a separate market named *Q*, the central and ISO-dependent reactive power scheduling is responsible for the reactive power support.

(3) A SC_k is also responsible for a portion of transmission losses resulting from consuming reactive power support, which introduces reactive power flows.

5.2.2 Step-wise procedures for decomposition

We derive the decomposition equations on a general power system with *N*-buses and *L*-branches. To simplify our presentation, we assume only two market players in the system: PX is a central power exchange market; and TX is a bilateral transaction. These

assumptions will be relaxed later. A system-wide reactive power market Q conducted by the ISO is responsible for overall reactive support services.

Step1: Select an appropriate angle for the slack bus from the given power flow solution, referring to equation (5.6).

Step 2: Decompose the nodal current vector based on TXs.

From a known operating point (V,θ), the (n×1) nodal current vector I_{bus} is determined by:

$$I_{bus} = [Y_{bus}] \times E_{bus} \quad \text{, where } E_{bus} = \begin{bmatrix} V_1 e^{j\theta_i} \\ . \\ V_n e^{j\theta_i} \end{bmatrix} \tag{5.7}$$

where Y_{bus} is the (n×n) nodal admittance matrix, which is nonsingular in consideration of line charging and other shunt terms.

According to the proposed approximation equation (5.3), I_{bus} is decomposed into individual market components. That is,

$$I_{PX} = \begin{bmatrix} . \\ \dfrac{P_{G,i}^{PX} - P_{D,i}^{PX}}{V_i \cos\theta_i} \\ . \\ . \\ \dfrac{P_{G,n}^{PX} - P_{D,n}^{PX}}{V_n \cos\theta_n} \end{bmatrix} \qquad I_{TX} = \begin{bmatrix} 0 \\ \dfrac{P_{G,k}^{TX}}{V_k \cos\theta_k} \\ 0 \\ \dfrac{-P_{D,m}^{TX}}{V_m \cos\theta_m} \\ 0 \end{bmatrix} \qquad I_Q = I_{bus} - I_{PX} - I_{TX} \tag{5.8}$$

where $P_{G,*}^{SC_k}, P_{D,*}^{SC_k}$ are the active power generations and loads at bus i, in association with PX or TX. TX is with the source and sink buses at k and m respectively.

Step 3: Decomposed nodal voltage components immediately follow from Step 2 by Kirchhoff Laws.

$$E_* = [Y_{bus}]^{-1} \times (I_*)^* \tag{5.9}$$

where the subscript symbol $*$ means PX, TX or Q individually. Normally,

$$|E_Q| \approx |E_{bus}| \approx 1 \qquad |E_{PX}| \approx 0 \qquad |E_{TX}| \approx 0 \tag{5.10}$$

Step 4: Compute branch current components $I_{*,i-j}, I_{*,j\_i}$ on any link between buses i and j by substituting the decomposed bus voltage vectors E_* of equation (5.9) into the branch current equations as follows.

In terms of a transmission line, or a transformer with a ratio 1.0, the decomposed branch current components directed from the buses i to j are derived by:

$$I_{*,i-j} = E_{*,i} b_{0,l} + (E_{*,i} - E_{*,j}) \times (g_{ij} + jb_{ij}) \tag{5.11}$$

$$I_{*,j-i} = E_{*,j} b_{0,l} + (E_{*,j} - E_{*,i}) \times (g_{ij} + jb_{ij}) \tag{5.12}$$

where b_l is the half line shunt susceptance. The symbol $*$ means PX, TX or Q individually.

For other branches, such as transformers with non-standard ratios (i.e., $t_{ij} \neq 1.0$), their branch currents can be derived easily.

Step 5: Decompose complex power flows over each branch.

For example, in terms of a branch between buses i and j, the complex power flow with respect to "from" bus of the branch is:

$$S_{i-j} = E_{bus,i} \times I_{i-j}^{*} \tag{5.13}$$

Further, it can be rewritten as

$$\begin{aligned} S_{i-j} &= (E_{Q,i} + E_{PX,i} + E_{TX,i}) \times (I_{Q,i-j} + I_{PX,i-j} + I_{TX,i-j})^{*} \\ &= (E_{Q,i} + E_{PX,i}) I_{PX,i-j}^{*} \overset{\text{1st term}}{\hookleftarrow} + (E_{Q,i} + E_{TX,i}) I_{TX,i-j}^{*} \overset{\text{2nd term}}{\hookleftarrow} \\ &+ E_{Q,i} I_{Q,i-j}^{*} \overset{\text{3rd term}}{\hookleftarrow} + (E_{PX,i-j} I_{TX,i-j}^{*} + E_{TX,i} I_{PX,i-j}^{*}) \overset{\text{4th term}}{\hookleftarrow} \\ &+ E_{PX,i} I_{Q,i-j}^{*} \overset{\text{5th term}}{\hookleftarrow} + E_{TX,i} I_{Q,i-j}^{*} \overset{\text{6th term}}{\hookleftarrow} \end{aligned} \tag{5.14}$$

where $E_{bus,i}, E_{PX,i}, E_{TX,i}, E_{Q,i}$ is the i^{th} element of the voltage vectors $E_{bus}, E_{PX}, E_{TX}, E_Q$ individually.

We categorize terms of equation (5.14) as follows:

- The 1st, 2nd and 3rd terms are major components attributed to PX, TX and Q markets respectively.
- The 4th term represents an interacting component between energy markets PX and TX.

- The 5th and 6th terms represent interacting component between PX/TX and *Q* markets separately.

Evidently, the market players PX and TX account for self-induced terms, and also take care of the interacting cross-terms. Moreover, there is a flexibility to allocate the interactive component between PX and TX, which can be designed into market rules. Therefore, we the complex flow decomposition equation for one branch directed from i to j as follows.

$$S_{i-j} = S_{PX,i-j} + S_{TX,i-j} + S_{Q,i-j} \tag{5.15}$$

where

$$S_{PX,i-j} = (E_{Q,i} + E_{PX,i}) \times I^*_{PX,i-j} + E_{PX,i} I^*_{Q,i-j} + f_{PX\omega TX} \times (E_{PX,i} I^*_{TX,i-j} + E_{TX,i} I^*_{PX,i-j})$$

$$S_{TX,i-j} = (E_{Q,i} + E_{TX,i}) \times I^*_{TX,i-j} + E_{TX,i} I^*_{Q,i-j} + f_{TX\omega TX} \times (E_{TX,i} I^*_{PX,i-j} + E_{TX,i} I^*_{PX,i-j})$$

$$S_{Q,i-j} = E_{Q,i} I^*_{Q,i-j}$$

$f_{PX\omega TX}, f_{TX\omega PX}$ are sharing factors imposed upon PX and TX for their interactive component. $f_{PX\omega TX} + f_{TX\omega PX} \equiv 1.$

Along the same line, the complex power flow with respect to "to" bus of the branch can be decomposed into the following market components:

$$S_{j-i} = S_{PX,j-i} + S_{TX,j-i} + S_{Q,j-i} \tag{5.16}$$

where

$$S_{PX,i-j} = (E_{Q,i} + E_{PX,i}) \times I^*_{PX,i-j} + E_{PX,i} I^*_{Q,i-j} + f_{PX\omega TX} \times (E_{PX,i} I^*_{TX,i-j} + E_{TX,i} I^*_{PX,i-j})$$
$$S_{TX,i-j} = (E_{Q,i} + E_{TX,i}) \times I^*_{TX,i-j} + E_{TX,i} I^*_{Q,i-j} + f_{TX\omega PX} \times (E_{PX,i} I^*_{TX,i-j} + E_{TX,i} I^*_{PX,i-j})$$

$$S_{Q,j-i} = E_{Q,j} I^*_{Q,i-j}$$

Further, the decomposed real flow, real loss, reactive flow and reactive loss components on the branch immediately follow from the solved complex power flow components $S_{*,i-j}, S_{*,j-i}$. In particular,

$$P_{flow(*),i-j} = \frac{1}{2}\mathrm{Re}(S_{*,i-j} - S_{*,j-i}) \tag{5.17}$$

$$P_{loss(*),i-j} = \mathrm{Re}(S_{*,i-j} + S_{*,j-i}) \tag{5.18}$$

$$Q_{flow_{(*),i-j}} = \frac{1}{2}\mathrm{Im}(S_{*,i-j} - S_{*,j-i}) \tag{5.19}$$

$$Q_{loss(*),i-j} = \mathrm{Im}(S_{*,i-j} - S_{*,j-i}) \tag{5.20}$$

where * means PX, TX or Q individually.

Step 6: Distribute the portion of transmission loss arising from reactive power delivery to the energy customers in proportion to their reactive power usage.

The intent of reactive power scheduling is to balance the system reactive loads and MVAr losses mainly generated from interzonal power transfers. The transmission losses incurred from reactive power flows only takes up a small percent of the system losses under normal operating conditions. Therefore, we reallocate it between PX and TX in proportion to their reactive power usage.

$$\Delta P_{L(*,Q)} = \frac{\sum_{i\in N} Q_{D*,i} + \sum_{L} Q_{loss(*),i-j}}{\sum_{k=PX,TX}\left(\sum_{i\in N} Q_{Dk,i} + \sum_{L} Q_{loss(k),i-j}\right)} \times \sum_{L} P_{loss(Q),i-j} \tag{5.21}$$

where * denotes energy interchange schedules PX or TX.

Eventually, the transmission loss charges to PX and TX are:

$$P_{L(PX)} = \sum_{L} P_{loss(PX),i-j} + \Delta P_{L(PX,Q)} \tag{5.22}$$

$$P_{L(TX)} = \sum_{L} P_{loss(TX),i-j} + \Delta P_{L(TX,Q)} \tag{5.23}$$

Thus, all transmission losses are distributed among energy transactions independent of the reactive power market clearing system.

Step 7: Adjust loss shares among the market players by an iteration scheme.

As only a relatively small number of generators are used for load following purposes in a power system, the loss generated from a PX or a bilateral transaction is likely to be supplied by a third party, not necessarily the same generator serving the load. Accordingly, an adjustment process is needed to take care of the loss. For example, suppose TX decides to buy the loss from a third party generator (say s), then a small

amount of generation from the supplier s is attributed to the TX, which corresponds to the allocated loss reflected in equation 5.23. We adjust the current vector I_{TX} accordingly, and repeat Steps 2 through 6 again. This adjustment scheme can be extended for a PX market similarly. Under normal operating conditions, the loss adjustment process converges in a few iterations.

It is straightforward to generalize to cases with a large number of the TXs. For any SC_k, the complex power flow contributions to one branch between the buses i and j are:

$$S_{SC_k,i-j} = (E_{Q,i} + E_{SC_k,i}) \times I_{SC_k,i-j} + E_{SC_k,i} I_{Q,i-j} + \sum_{h \in T-k} f_{SC_k \omega SC_h} \times (E_{SC_k,i} I_{SC_h,i-j} + E_{SC_h,i} I_{SC_k,i-j}) \quad (5.24)$$

and

$$S_{SC_k,j-i} = (E_{Q,j} + E_{SC_k,j}) \times I_{SC_k,j-i} + E_{SC_k,j} I_{Q,j-i} + \sum_{h \in T-k} f_{SC_k \omega SC_h} \times (E_{SC_k,j} I_{SC_h,j-i} + E_{SC_h,j} I_{SC_k,j-i}) \quad (5.25)$$

where T is the number of all energy scheduling coordinators including all the TXs and PXs.

5.3 Transaction-based voltage security margin allocation algorithm

Integrating the TBPF [10] and the index L would lead to a transaction-based voltage security utilization algorithm [5] that is formulated in the following section.

To simplify our presentation, we assume only two types of market players in the system: PX represents one central power exchange market, and TX represents a set of N_T bilateral transactions. A system-wide reactive power market Q conducted by the ISO is responsible for overall reactive support services.

Step 1: Decompose the nodal current vector based on TXs.

$$I_{bus} = [Y_{bus}] \times E_{bus} \text{ , where } E_{bus} = \begin{bmatrix} V_1 e^{j\theta_i} \\ . \\ V_n e^{j\theta_i} \end{bmatrix} \quad (5.26)$$

$$I_{PX} = \begin{bmatrix} \vdots \\ \dfrac{P_{G,i}^{PX} - P_{D,i}^{PX}}{V_i \cos\theta_i} \\ \vdots \\ \dfrac{P_{G,n}^{PX} - P_{D,n}^{PX}}{V_n \cos\theta_n} \end{bmatrix} \qquad I_{TX}^{(j)} = \begin{bmatrix} 0 \\ \dfrac{P_{G,k}^{TX(j)}}{V_k \cos\theta_k} \\ 0 \\ \dfrac{-P_{D,m}^{TX(j)}}{V_m \cos\theta_m} \\ 0 \end{bmatrix} \qquad j = 1,....,N_T$$

$$I_Q = I_{bus} - I_{PX} - \sum_{j=1}^{N_T} I_{TX}^{(j)} \tag{5.27}$$

where $P_{G,*}^{SC_k}, P_{D,*}^{SC_k}$ are the active power generation and load at bus i, in association with PX or TX. TX is with the source and sink buses at k and m respectively. N_T is the number of bilateral transactions.

Step 2: Decompose nodal voltage components

$$E_{TX}^{(j)} = [Y_{bus}]^{-1} \times (I_{TX}^{(j)})^* \quad j = 1,....,N_T$$

$$E_{PX} = [Y_{bus}]^{-1} \times (I_{PX})^* \tag{5.28}$$

$$E_Q = [Y_{bus}]^{-1} \times (I_Q)^*$$

All of the vectors above are of length N, corresponding to the N bus system.

The relationship between the bus voltages and these decomposed components of voltage is given by

$$E_{bus} = \left[\sum_{j=1}^{N_t} E_{TX}^{(j)} \right] + E_{PX} + E_Q \tag{5.29}$$

Step 3: Evaluating index L based on the decomposed voltage components.

$$S_{TX}^{(j)} = \begin{bmatrix} 0 \\ 0 \\ 0 \\ -P_d^{(j)} - jQ_d^{(j)} \\ 0 \end{bmatrix} \quad j = 1,....,N_T \tag{5.30}$$

$$S_{PX} = \begin{bmatrix} -P_{d_1} - jQ_{d_1} \\ . \\ . \\ . \\ -P_{d_n} - jQ_{d_n} \end{bmatrix} \tag{5.31}$$

Considering PX transaction as the first one, the index L is given by the following expression:

$$L_j^{PX} = \left| \frac{\overset{*}{S}_{j+}}{Y_{jj+} \left| V_{PX\,j} \right|^2} \right| , \tag{5.32}$$

where $S_{j+} = S_{PX\,j} + S_{jcorr}$, $\quad S_{jcorr} = \left(\sum_{\substack{i \in L \\ i \neq j}} \frac{\overset{*}{Z}_{ji}}{\overset{*}{Z}_{jj}} \frac{S_{PX\,i}}{V_{PX\,i}} \right) V_{PX\,j}$, $\quad Y_{jj+} = \frac{1}{Z_{jj}}$

and $V_{PX} = E_{PX} + E_Q$.

Here j represents all the load buses.

By reflecting the appropriate changes in the S_{j+} and V_{PX} terms of the previous expression, the index can be evaluated after adding each bilateral transaction TX one after the other. For example, the index after adding the first transaction TX to the PX would be given by

$$L_j^{PX+TX^{(1)}} = \left| \frac{\overset{*}{S}_{j+}}{Y_{jj+} \left| V_{(PX+TX^{(1)})\,j} \right|^2} \right| , \tag{5.33}$$

where $S_{j+} = S_{PX\,j} + S_{TX^{(1)}\,j} + S_{jcorr}$, $S_{jcorr} = \left(\sum_{\substack{i \in L \\ i \neq j}} \frac{\overset{*}{Z}_{ji}}{\overset{*}{Z}_{jj}} \frac{S_{PX\,i}}{V_{(PX+TX^{(1)})\,i}} \right) V_{(PX+TX^{(1)})\,j}$,

and $V_{(PX+TX^{(1)})} = E_{PX} + E_Q + E_{TX}^{(1)}$.

5.3.1 Test case for demonstrating the voltage security margin allocation algorithm

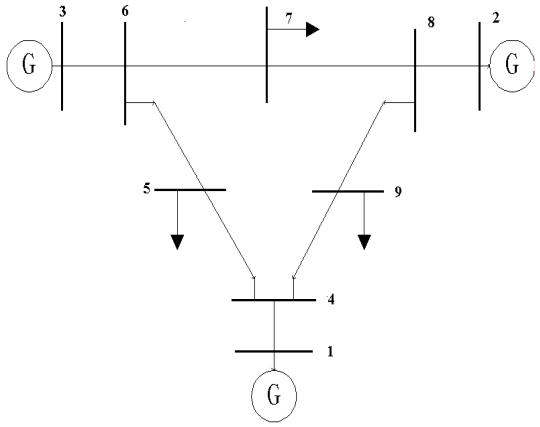

Figure 5-1 Test case for demonstration

Table 5-1 gives the details of the system. Table 5-2 gives the power data for the three transactions. Figure 5-2 gives the overall picture. After applying the voltage margin allocation algorithm, the decomposed bus voltage components are given in Table 5-3.

Line	Resistance (p.u)	Reactance (p.u)	Susceptance (p.u)	MVA Rating
1-4	0.0000	0.0576	0.0000	250
4-5	0.0170	0.0920	0.1580	250
5-6	0.0390	0.1700	0.3580	150
3-6	0.0000	0.0586	0.0000	300
6-7	0.0119	0.1008	0.2090	150
7-8	0.0085	0.0720	0.1490	250
8-2	0.0000	0.0625	0.0000	250
8-9	0.0320	0.1610	0.3060	250
9-4	0.0100	0.0850	0.1760	250

Table 5-1 Transmission line data

Bus No.	Pg1	Pd1	Qd1	Pg2	Pd2	Qd2	Pg3	Pd3	Qd3
1	67	0	0	50	0	0	0	0	0
2	163	0	0	0	0	0	0	0	0
3	85	0	0	0	0	0	50	0	0
4	0	0	0	0	0	0	0	0	0
5	0	90	30	0	0	0	0	50	0
6	0	0	0	0	0	0	0	0	0
7	0	100	35	0	0	0	0	0	0
8	0	0	0	0	0	0	0	0	0
9	0	125	50	0	50	0	0	0	0

Table 5-2 Power data for three transactions

Transaction 1 is the PX market operation with Bus 2 associated as the loss bus. Transaction 2 represents TX of firm power transfer of 50MW from bus 1 to bus 9. Transaction 3 represents TX of firm power transfer of 50MW from bus 3 to bus 5.

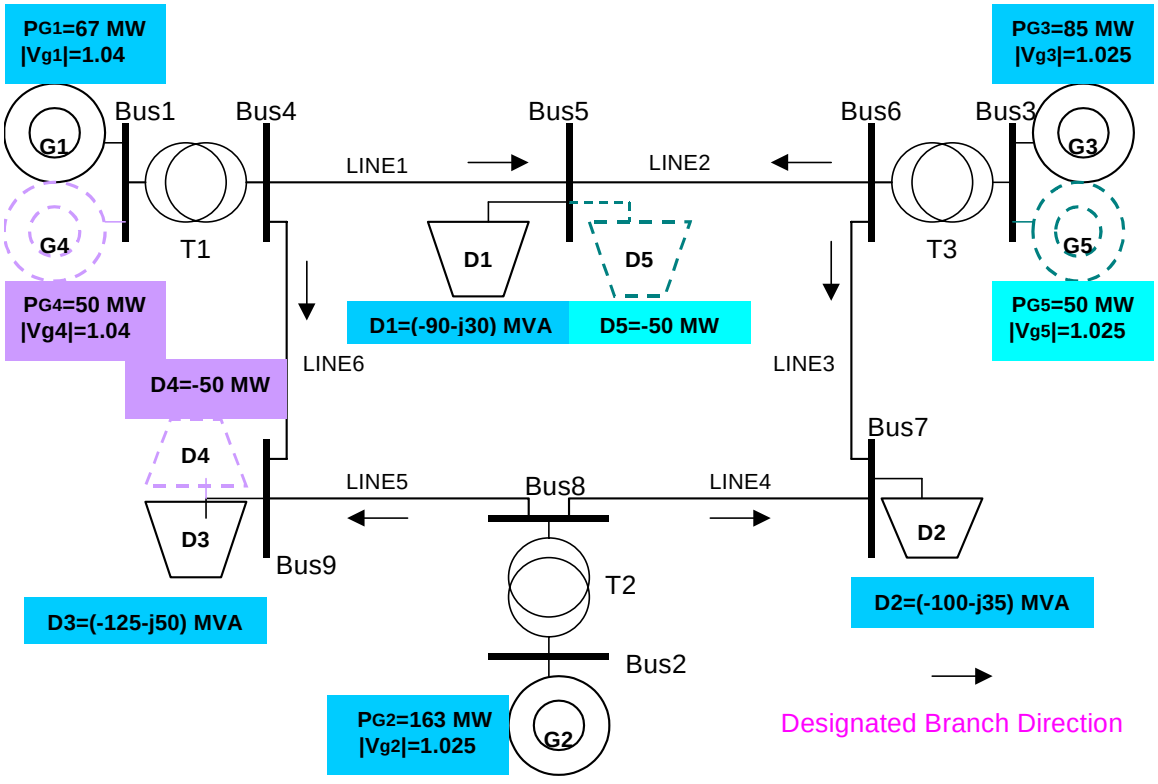

The WSCC 9 Bus Test System with 1 PX and 2 TX

Figure 5-2 The WSCC 9 bus test system with transactions

	PX	TX-1	TX-2	*Q*	System
Bus-1	0.0182	0.0539	0.0464	1.0507	1.0400
Bus-2	0.1644	0.0008	0.0149	1.0183	1.0250
Bus-3	0.0775	0.0110	0.0397	1.0180	1.0250
Bus-4	0.0530	0.0263	0.0464	1.0160	1.0173
Bus-5	0.0785	0.0213	0.0572	0.9922	0.9956
Bus-6	0.0303	0.0110	0.0111	1.0166	1.0286
Bus-7	0.0110	0.0047	0.0067	0.9997	1.0117
Bus-8	0.0631	0.0008	0.0149	1.0096	1.0214
Bus-9	0.0834	0.0105	0.0359	0.9721	0.9806

Table 5-3 Decomposed bus voltage components ($|V_*|$)

5.3.2 Results for various scenarios

Case I: Apply transaction-based voltage security margin algorithm

Transaction	Bus 4	Bus 5	Bus 6	Bus 7	Bus 8	Bus 9
1	0.0815	0.1346	0.0559	0.1087	0.0682	0.1616
1+2	0.0972	0.1471	0.0604	0.1167	0.0784	0.2046
1+2+3	0.1111	0.1892	0.0693	0.1222	0.0821	0.2137

Table 5-4 Results for Case I

Observations for Case I

1) Node-wise voltage stability margin utilization, for all bilateral transactions existing in the market is obtained by this procedure.

2) The index at the bus where the transaction takes place is affected the most, which is as expected.

3) The effect of individual transactions on other load buses can also be computed by this algorithm.

Case II: To study the effect of changing the sequence of the transactions

For the same data as in Case I, we changed the sequence of transactions 2 and 3 and re-evaluated the indices.

Transaction	Bus 4	Bus 5	Bus 6	Bus 7	Bus 8	Bus 9
1	0.0815	0.1346	0.0559	0.1087	0.0682	0.1616
1+3	0.0952	0.1761	0.0647	0.1142	0.0720	0.1711
1+2+3	0.1111	0.1892	0.0693	0.1222	0.0821	0.2137

Table 5-5 Results for Case II

Observations for Case II

1) The change in the index at the load buses corresponding to the transaction is not affected much by the change in the transaction sequence.

2) Other cases should be studied to come out with a definite conclusion.

Case III: Effect of a contingency

We choose Line 4-9 outage as the contingency. Let the two transactions be as follows:

Transaction 2: 100 +j 50 MVA TX between bus 2 and 7.
Transaction 3: 10 MW firm power between bus 3 and 5.

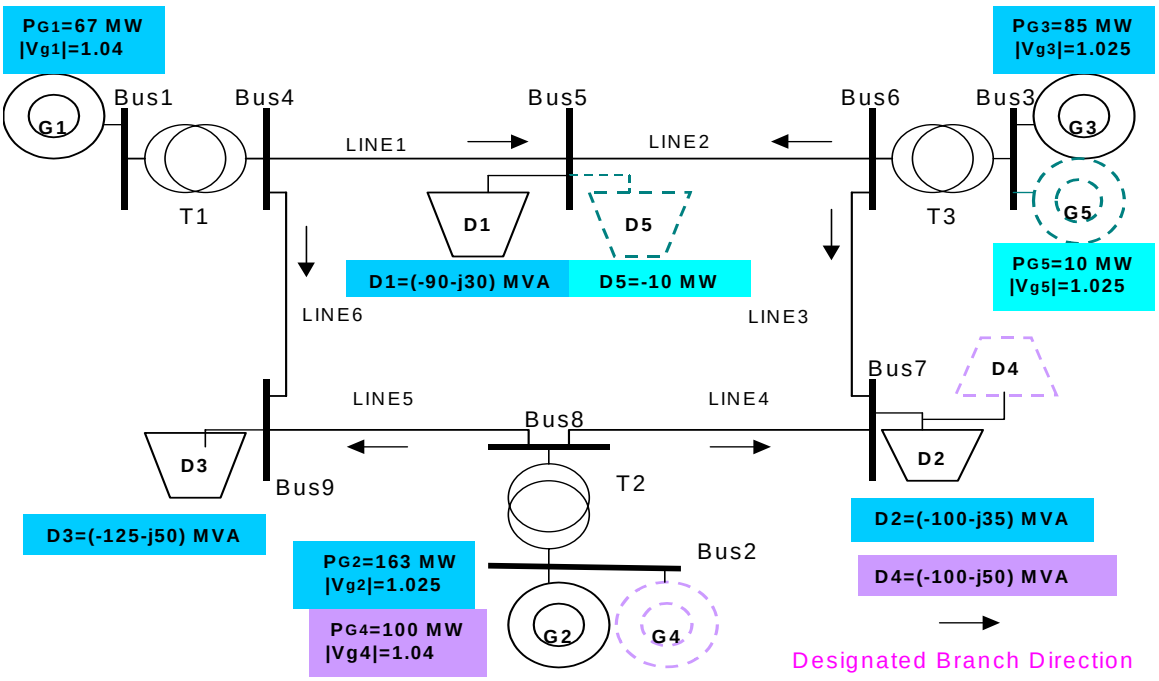

The WSCC 9 Bus Test System with 1 PX and 2 TX

Fig 5-3 Transaction pattern for Case III

Transaction	Bus 4	Bus 5	Bus 6	Bus 7	Bus 8	Bus 9
1	0.0417	0.1119	0.0719	0.1879	0.1653	0.7093
1+2	0.0473	0.1269	0.1036	0.2924	0.2199	0.8427
1+2+3	0.0504	0.1351	0.1053	0.2932	0.2201	0.8428

Table 5-7 Indices evaluated after the contingency

Transaction	Bus 4	Bus 5	Bus 6	Bus 7	Bus 8	Bus 9
1	0.0908	0.1428	0.0610	0.1253	0.0775	0.1868
1+2	0.1009	0.1591	0.0882	0.2097	0.1127	0.2074
1+2+3	0.1034	0.1669	0.0898	0.2105	0.1133	0.2088

Table 5-8 Indices evaluated before contingency

Observations for Case III

1) The transaction at bus 7 has an effect on the bus 9 index, as seen in Table 5-8.

2) The above effect is magnified in the case of a contingency, also as seen from Table 5-7. Bus 9 is driven closer to voltage collapse as the index has reached 0.8427 after transaction 2.

3) This seems to be because bus 9 has now lost reactive support from generator 1 following the contingency.

Case IV: Study the effect of power factor of load

(a) Let the transaction pattern for 2 and 3 be as follows:

Transaction 2: Firm power transfer of 50 MW from bus 1 to 9.
Transaction 3: 145 + j180 MVA transfer between bus 5 and generator at bus 3.

Transaction	Bus 4	Bus 5	Bus 6	Bus 7	Bus 8	Bus 9
1	0.0919	0.2150	0.0623	0.1085	0.0682	0.1666
1+2	0.1146	0.2518	0.0704	0.1216	0.0813	0.2184
1+2+3	0.2545	0.7826	0.1498	0.1874	0.1251	0.3616

Table 5-9 Results for case IV(a)

(b) Let the transaction pattern for 2 and 3 be as follows:

Transaction 2: Firm power transfer of 50 MW from bus 1 to 9
Transaction 3: 145 + j90 MVA transfer between bus 5 and generator at bus 3

Transaction	Bus 4	Bus 5	Bus 6	Bus 7	Bus 8	Bus 9
1	0.0928	0.1775	0.0627	0.1164	0.0730	0.1786
1+2	0.1116	0.1961	0.0683	0.1262	0.0845	0.2279
1+2+3	0.1755	0.4029	0.1072	0.1539	0.1030	0.2798

Table 5-10 Results for Case IV(b)

Observations for Case IV

1) It can be seen from Tables 5-9 and 5-10 that the index evaluated for the same real power transfer but with a more lagging power factor is larger, which reflects correctly the voltage stability margin sensitivity to reactive demand of load.

2) Though the load power factor is changed at bus 5, the index at load buses 7 and 9 are affected significantly.

Case V: Study the location of the generator in the transactions

(a) Let the transaction pattern for 2 and 3 be as follows:

Transaction 2: Firm power transfer of 50 MW from generator at bus 1 to bus 9.
Transaction 3: 145 + j90 MVA transfer between bus 5 and generator at bus 1.

Transaction	Bus 4	Bus 5	Bus 6	Bus 7	Bus 8	Bus 9
1	0.0851	0.1576	0.0576	0.1083	0.0681	0.1615
1+2	0.1009	0.1735	0.0626	0.1170	0.0785	0.2047
1+2+3	0.1693	0.3803	0.1040	0.1500	0.1004	0.2684

Table 5-11 Results for Case V(a)

(b) Let the transaction pattern for 2 and 3 be as follows:

Transaction 2: Firm power transfer of 50 MW from generator at bus 1 to bus 9.
Transaction 3: 145 + j90 MVA transfer between bus 5 and generator at bus 3.

Transaction	Bus 4	Bus 5	Bus 6	Bus 7	Bus 8	Bus 9
1	0.0928	0.1775	0.0627	0.1164	0.0730	0.1786
1+2	0.1116	0.1961	0.0683	0.1262	0.0845	0.2279
1+2+3	0.1755	0.4029	0.1072	0.1539	0.1030	0.2798

Table 5-12 Results for Case V(b)

Observation for Case V

Referring to Tables 5-11 and 5-12, conducting a transaction from a nearby generator causes a smaller index. A shorter line is the reason for this.

5.4 Publications

The detailed summary and application scopes of the transaction-based voltage margin allocation algorithm can be obtained from reference [5].

The formulation of the transaction-based power flow with numerical examples has been detailed in reference [10]. This new algorithm has been applied to effectively address the issue of equitable loss allocation in power markets [11]. The application scope of transaction-based power flow in formulating a congestion management policy has been detailed in reference [9].

One of the objectives of this project was to formulate a basis for evaluating the utilization factors and the pricing of control elements in a market-based power system, within the context of voltage stability. Using the bifurcation analysis a procedure to allocate contribution of generators, transmission and control elements in voltage stability has been evolved [6]. The authors feel that this procedure could be extended in evolving an equitable utilization factor policy for the various control elements in power system operation.

6
Bifurcation Analysis for Voltage Stability Margin Evaluation

Thus far we have focused on the static voltage stability margin and have pointed out its potential limitations. Now we will demonstrate its limitations by looking at dynamic stability margin and find the relationships between these two margins. Our preliminary study successfully explains why the dynamic stability margin is equal or less than the steady-state stability margin; and the smaller of the two is the valid stability margin, which should be used to gauge the stability margin. Bifurcation analysis is used to calculate the dynamic stability margin, while power flow analysis is used to calculate the steady-state stability margin.

Dynamic analysis is more time-consuming and difficult than steady-state analysis. For this reason, steady-state analysis has been used to estimate the stability margin. However, when the dynamic stability margin is much smaller than the steady-state margin, dynamic analysis has to be used to obtain the valid margin. Therefore, an important issue is to determine when a steady-state analysis is good enough to estimate the stability margin as shown by a simple example in section 6.2.

For market-based power systems, it is important to know who contributes to avoiding a voltage collapse, where this contribution could come from different parts of the power system: generators, control systems and transmission elements, etc. Here we focus on how to allocate the responsibility and contribution by using bifurcation analysis. We investigate how parameters of the system influence the bifurcation points. Three bifurcations (that is, the singularity induced bifurcation, saddle-node and Hopf bifurcations [6]), and their relationship to several commonly used controllers, [6] are analyzed. Their parameters' impact on the bifurcation points is investigated, from which we find a way to allocate the contribution by analyzing the relative positions of the bifurcations.

There are physical limits on power system components; here we focus on deciding the size of the exciter, which has a significant influence on voltage stability. Analyzing the impacts of exciter size will benefit system design and the allocation of the responsibility of the voltage collapse in a market-based environment.

The load model also has a great impact on voltage stability. We will show how different load patterns influence the bifurcation point, and thus the stability margin.

In this chapter, we use a simple two-bus system shown in Figure 6-1 to demonstrate our approach. In this simple system, we assume that the voltage dynamic is decoupled from the angle dynamic, which is assumed to be well behaving, so the angle dynamic can be ignored in this scenario.

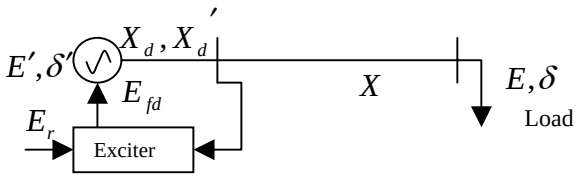

Figure 6-1 The simple two-bus system

6.1 Introduction

The dynamics of this system can be modeled by parameter-dependent, differential-algebraic equations [6] as:

$$\dot{x} = f(x, y, p), \quad f : \Re^{n+m+q} \to \Re^n \tag{6-1}$$

$$0 = g(x, y, p), \quad g : \Re^{n+m+q} \to \Re^m \tag{6-2}$$

$$x \in X \subset \Re^n, \quad y \in Y \subset \Re^m, \quad p \in P \subset \Re^q$$

The differential equation (6-1) represents the exciter dynamics and its control system, and the algebraic equation (6-2) represents the load flow equation. Here we focus on three commonly used controllers (that is, the P-controller, PI-controller and PID controller of a voltage regulator). The load flow equation of this system and the mathematical model of these three types of controller will be introduced.

The reduced Jacobian matrix of the system can be written as:

$$F_x = \left[f_x - f_y g_y^{-1} g_x \right] \tag{6-3}$$

Through the analysis of the eigenvalue of F_x, we can demonstrate the influence of the control system. We observed that three types of bifurcation usually occurred: Hopf bifurcation, saddle-node and singularity induced bifurcation. Correspondingly, we denote these three types of bifurcation as A, B and C. Then, we show how different controllers and their parameters impact on the locations of A, B and C on the PV curve.

Now we introduce the models as follows:

6.1.1 Algebraic equations of load flow [6]

$$\begin{cases} P = \dfrac{E' E}{x'} \sin \delta' \\ Q = \dfrac{-E^2 + EE' \cos \delta'}{x'} \end{cases} \tag{6-4}$$

$$\begin{cases} P = \dfrac{E_G E}{x} \sin \delta_G \\ Q = \dfrac{-E^2 + E E_G \cos \delta_G}{x} \end{cases} \tag{6-5}$$

Equation (4) can be simplified as:

$$0 = E'^2 E^2 - (x'P)^2 - (x'Q + E^2)^2 \tag{6-6}$$

Here equation (6-6) is the g(x,y,p) in equation (6-2).

6.1.2 Differential equations of controllers

The mathematic models of the three controllers are given in this section.

1) P-controller:

$$\dot{E}' = \frac{1}{T'_{d0}} \cdot \left[-\frac{x + x_d}{x'} E' + \frac{x_d - x'_d}{x'} \cdot \frac{(E^2 + x'Q)}{E'} + E_{fd} \right] \tag{6-7}$$

$$\dot{E}'_{fd} = \frac{1}{T} \left\{ -(E_{fd} - E^0_{fd}) - K_P \left[\frac{1}{E} \sqrt{(xP)^2 + (xQ + E^2)^2} - E_r \right] \right\} \tag{6-8}$$

Here equations (6-7) and (6-8) are the f(x,y,p) in equation (6-1).

2) PI-controller

$$\dot{E}' = \frac{1}{T'_{d0}} \cdot \left[-\frac{x + x_d}{x'} E' + \frac{x_d - x'_d}{x'} \cdot \frac{(E^2 + x'Q)}{E'} + E_{fd} \right] \tag{6-9}$$

$$\dot{E}_{fd} = \frac{1}{T} \left\{ -(E_{fd} - E^0_{fd}) - E_{PI} / T_I - K_P \left(\frac{1}{E} \sqrt{(xP)^2 + (xQ + E^2)^2} - E_r \right) \right\} \tag{6-10}$$

$$\dot{E}_{PI} = \frac{1}{E} \sqrt{(xP)^2 + (xQ + E^2)^2} - E_r \tag{6-11}$$

Here, equations (6-9) to (6-11) are the f(x,y,p) in equation (6-1).

3) PID-controller

For a PID controller [6],

$$K_P + \frac{1}{T_I s} + K_D s \tag{6-12}$$

We know that a D-controller is not practical due to noises, so if T_D is small enough, we can use equation (6-13) to replace equation (6-12):

$$K_P + \frac{1}{T_I s} + \frac{K_D s}{1 + T_D s} \tag{6-13}$$

Then, the control system can be expressed as below:

$$\dot{E}' = \frac{1}{T_{d0}'} \cdot \left[-\frac{x + x_d}{x'} E' + \frac{x_d - x_d'}{x'} \cdot \frac{(E^2 + x'Q)}{E'} + E_{fd} \right] \tag{6-14}$$

$$\dot{E}_{fd} = \frac{1}{T} \left\{ -(E_{fd} - E_{fd}^0) - E_{PI} / T_I - E_D - (K_P + \frac{K_D}{T_D})(\frac{1}{E}\sqrt{(xP)^2 + (xQ + E^2)^2} - E_r) \right\} \tag{6-15}$$

$$\dot{E}_{PI} = \frac{1}{E}\sqrt{(xP)^2 + (xQ + E^2)^2} - E_r \tag{6-16}$$

$$\dot{E}_D = -\frac{K_D}{T_D^2}(\frac{1}{E}\sqrt{(xP)^2 + (xQ + E^2)^2} - E_r) - \frac{E_D}{T_D} \tag{6-17}$$

Here equations (6-14) to (6-17) are the f(x,y,p) in equation (6-1).

6.2 Dynamic stability margin vs. static stability margin

Dynamic stability margin is equal to or less than steady-state stability margin. The smaller of the two is the valid stability margin. Bifurcation analysis is used to calculate the dynamic stability margin, which is time-consuming and more difficult than steady-state analysis. If we can determine when the steady-state analysis is good enough to estimate the stability margin, we can avoid the unneeded computations. We will discuss this issue in section 6.6 based on this simple two-bus system.

Here we use a simple example in reference [12] to show that the dynamic stability margin is smaller than the static margin. The regulator used in this example is a P-regulator with constant E_{fd0}=1.6.

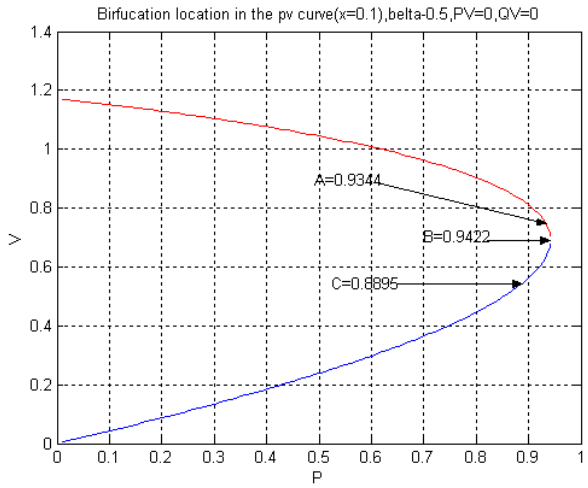

Figure 6-2 The locations of bifurcation points on PV curve

In the above figure, we found Hopf bifurcation point A in the upper part of the PV curve, which is the dynamic stability margin. We can see that P_A is smaller than the static margin P_B (here P_B=Pmax), when the system go beyond A point, the system will lose stability after a small disturbance, as shown below.

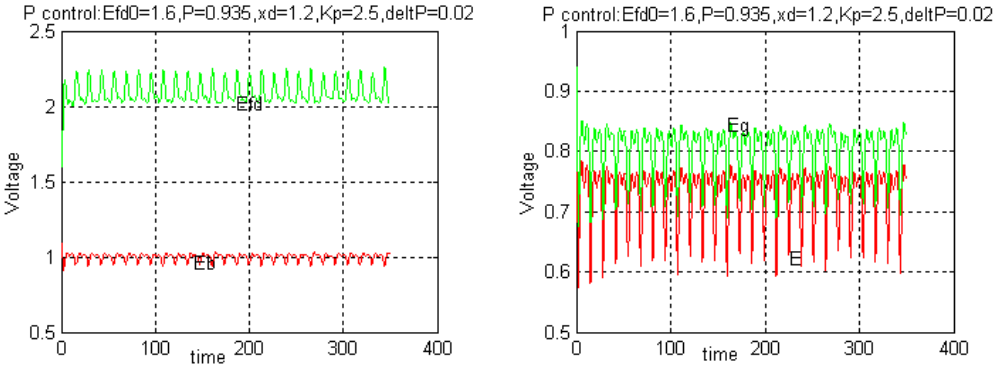

Figure 6-3 The Dynamic Response of Two-Bus System

When the system go beyond the A point, the system has a severe oscillation and cannot maintain stability. Therefore, we know that the dynamic margin A is the stability margin, which we need bifurcation analysis to find. The static margin B point is a too optimistic estimation .

6.3 Allocate the responsibility for voltage collapse with bifurcation analysis

In the following, we analyze the impacts of these controllers on the voltage stability of the system. Accordingly, we determine how to allocate the responsibility of voltage collapse. In this section, we assume constant load with a fixed power factor, and we have infinite exciter size. In all examples given in this section, we assume P=2Q.

6.3.1 On P-regulator

We note that this P-regulator reschedules E_{fd0} to keep $E_G \equiv E_r$.

Here we will show how K_p impacts on the locations of bifurcation points.

When K_p =2.5, 5, 10, the locations of the bifurcations A, B and C, and the eigenvalues of the reduced matrix are shown in Figures 6-4 to 6-6.

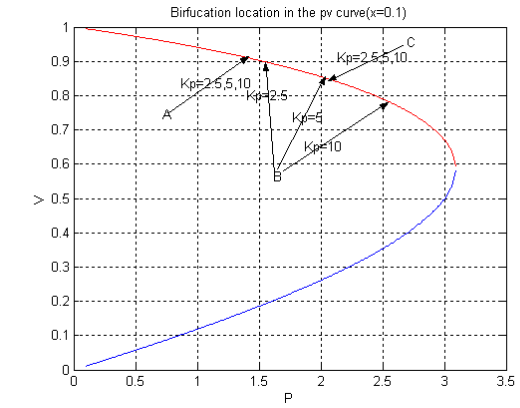

Figure 6-4 The locations of bifurcations points with Kp=2.5, 5, 10

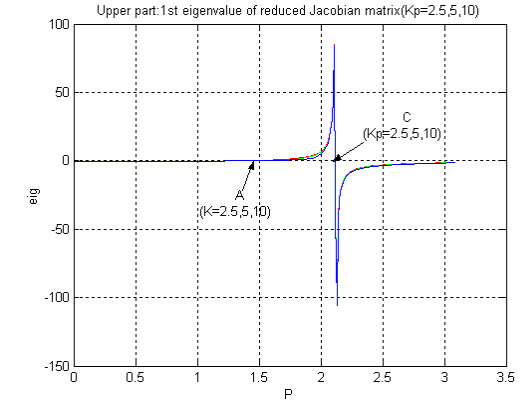

Figure 6-5 The eigenvalue which is slightly influenced by K_p

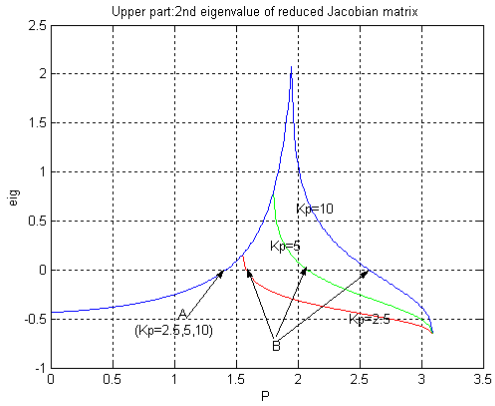

Figure 6-6 The eigenvalue which is strongly associated with K_p

By our calculations, with constant load and the infinite exciter size, bifurcation point C is only determined by the transmission system. It will not be influenced by the parameters of controller. However, point B will vary when K_p changes. B approaches Pmax when K_P goes to infinity. B>C when K_P>5.25. B ≈ A when K_P=1.895. When K_P<1.895, A will disappear. B approaches 0.735 when K_P approaches 0.

In Figure 6-5, note that K_p has little influence on one of the eigenvalues (denoted by EigT), while in Figure 6-6, K_p has a substantial impact on the other eigenvalue (denoted by EigC).

When K_p =1.8, Figure 6-9 shows the location of B and C in PV curve. A has disappeared. From Figures 6-4 to 6-9 we can see that the eigenvalue EigT is strongly related to the load flow, while the eigenvalue EigC is strongly influenced by the controller.

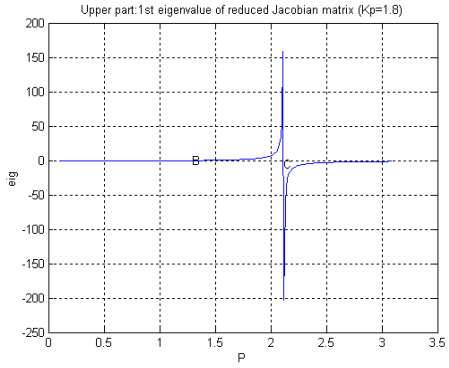

Figure 6-7 The curve of eigenvalue EigT when K_p=1.8

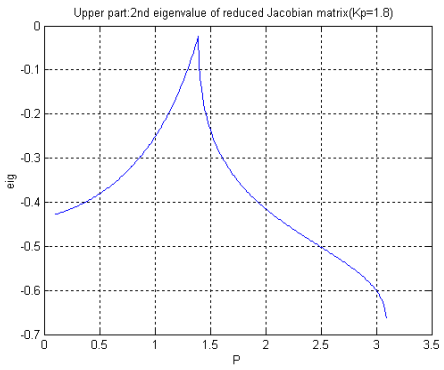

Figure 6-8 The curve of eigenvalue EigC when K_p=1.8

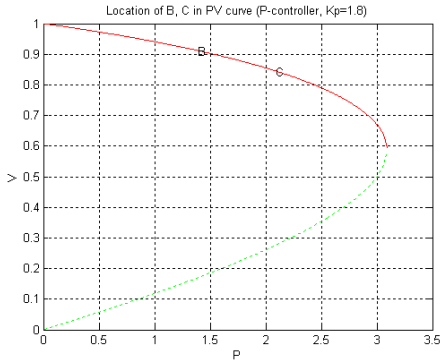

Figure 6-9 The location of B and C on PV Curve when K_p=1.8

We can conclude that there are three basic patterns:

1) $P_A<P_B<P_C$. When $P\in (P_A,P_B)$, both the eigenvalue EigT and EigC are positive; when $P\in (P_B,P_C)$, only the eigenvalue EigT is positive.

2) $P_A<P_C<P_B$. When $P\in (P_A,P_C)$, both the eigenvalue EigT and EigC are positive; when $P\in (P_C,P_B)$, only the eigenvalue EigC is positive.

3) Point A disappears and $P_B<P_C$. Only the eigenvalue EigT is positive when $P\in (P_B,P_C)$.

6.3.2 On PI- regulator

Several important parameters are given as: K_p =2.5, T_I =5.0/ T_I =20.

Using equation (3), (6) and (9) to (11), we can obtain three eigenvalues of the system: EigC (EigC is influenced by K_p and T_I, and is mainly influenced by T_I) and EigT. The other eigenvalue is always negative. We also found bifurcation points A, B and C.

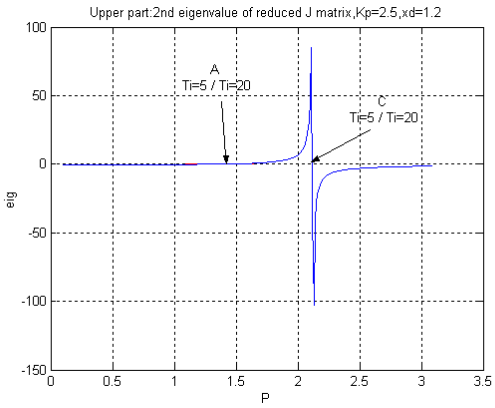

Figure 6-10 The curve of eigenvalue EigT (PI-Controller)

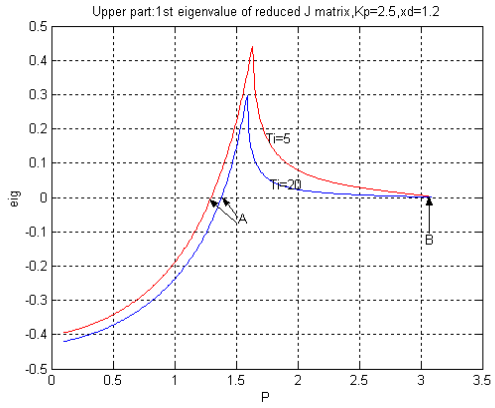

Figure 6-11 The curve of eigenvalue EigC (PI-Controller)

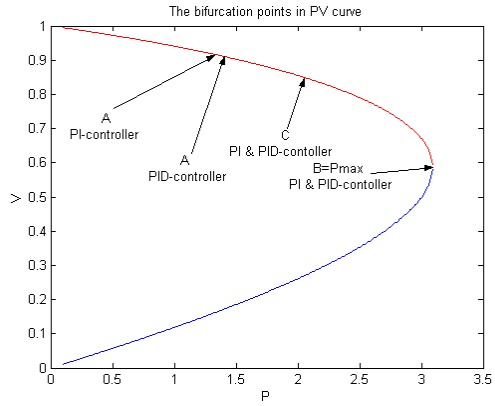

Figure 6-12 The location of A, B and C in PV curve for PI/PID controller

From Figures 6-10 to 6-12, we can conclude that PI controller behaves very much like the P-controller case as $K_P \to \infty$. When $P \in (0,P_A)$, all eigenvalues are negative; when $P \in (P_A,P_C)$, both eigenvalue EigC and EigT are positive; when $P \in (P_C,P_B)$, only the eigenvalue EigC is positive. Accordingly, it follows the basic pattern 2 as described in 6.3.1.

6.3.3 On PID-regulator

Several important parameters are given as: Kp=2.5, TI=5.0, K_D=1,T_D=0.01/ T_D =0.005. This kind of regulator behaves like a PI-controller. This follows the basic pattern 2 as discussed in 6.3.1.

Through sections 6.3.1, 6.3.2, and 6.3.3, given the constant load and infinite exciter size, we conclude that the three basic ordering patterns of bifurcation points A, B, and C (as discussed in 6.3.1) are generally true for all controllers which can keep $E_G \equiv E_r$. Our experience indicates that no other ordering of A, B, and C is possible. Accordingly, we can draw these conclusions.

1) $P_A<P_B<P_C$. When $P \in (P_A,P_B)$, both EigC and EigT are positive; and when $P \in (P_B,P_C)$, only the EigT is positive. From the parameter analysis, we conclude that the voltage collapse is due to both the controller and transmission when $P \in (P_A,P_B)$. The voltage collapse is only caused by the transmission part when $P \in (P_B,P_C)$. In this case, [P_A, P_C] is the unstable area, and P_A determinesthe dynamic stability margin.

2) $P_A<P_C<P_B$. When $P \in (P_A,P_C)$, both EigC and EigT are positive; and when $P \in (P_C,P_B)$, only the EigC is positive. From the parameter analysis we conclude that the voltage collapse is due to both the controller and transmission when $P \in (P_A,P_C)$. The voltage collapse is caused by the controller when $P \in (P_C,P_B)$. In this case, [P_A, P_B] is the unstable area, and P_A determines the dynamic stability margin.

3) Point A disappears and $P_B<P_C$, only the EigT is positive when $P \in (P_B,P_C)$. Thus, the voltage collapse is only due to transmission when $P \in (P_B,P_C)$. In this case, [P_B, P_C] is the unstable area, and P_B is the dynamic stability margin.

4) In conclusion, the tuning of the control parameters will influence P_A and P_B, thus, the dynamic stability margin of the system. This conclusion will also benefit the design of the system.

6.4 The influence of the exciter size on the bifurcation points

When the exciter is at its limit, its input, E_{fd}, will no longer be regulated with the change of the voltage. E_{fd} will be kept as E_{fd_max}. To demonstrate our analysis on the limit of the exciter, we draw two PV curves in Figure 6-13 and 6-14. The shorter nose curve denotes the system without regulation, which has a constant $E_{fd} = E_{fd\_max}$; the longer nose curve denotes the system with regulated E_{fd}. When the load increases, E_{fd} will be regulated to hit its limit E_{fd_max} at the D point (the intersection of the two PV curves), then the system will go along the PV curve with a shorter nose, which is shown by arrows in Figures 6-13 and 6-14. In this section, three widely used regulators are analyzied: P-regulator ($E_{fd}^{\ 0}$ is rescheduled to keep $E_G \equiv E_r$), PI-regulator and PID-regulator. Here we also assume that the load type is constant.

By comparing the PV curves and the locations of the bifurcation points, we found two basic patterns identified by whether the intersection point D is in upper part or lower part of the shorter nose PV curve. The two patterns are shown in Figure 6-13 and Figure 6-14 respectively:

1) Upper pattern: The intersection of two PV curves is in the upper part of the PV curve with shorter nose.

In this basic pattern, the possibilities of dynamic stability margin are given as following (For each point, says D, we associate D with P_D as the real load at point D.):

- If $P_A<P_D$, the dynamic stability margin is $P_{A.}$ (If A point disappears, P_B is the dynamic stability margin.).
- If $P_A> P_D$, the dynamic stability margin is $P_{B1.}$

For steady stability margin:

- If $P_C< P_D$, the steady-state margin is $P_{C.}$
- If $P_C > P_D$, the steady-state margin is P_{B1}.

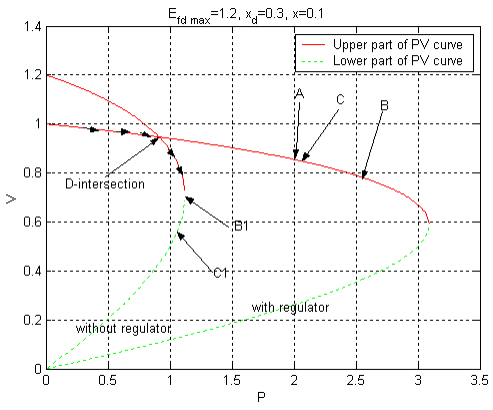

Figure 6-13 Upper pattern

2) Lower pattern: The intersection of two PV curves is in the lower part of the PV with shorter nose.

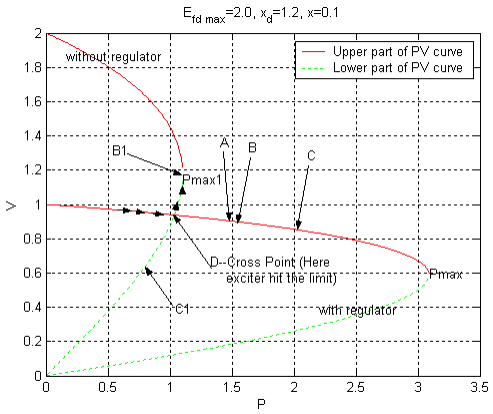

Figure 6-14 Lower pattern

In this basic pattern, the possibilities of dynamic stability margin are given as following.

- If $P_A<P_D$, the dynamic stability margin is P_A. (If A point disappears and $P_B<P_D$, P_B is the dynamic stability margin.)
- If $P_A>PD$ and $P_{C1}<P_D$, the dynamic stability margin is P_D.
- If $P_A>P_D$ and $P_{C1}>=P_D$, the dynamic stability margin is P_{C1}.

For the steady-state stability margin, there are also several possibilities.

- If $P_C<P_D$, the steady-state margin is P_C.
- If $P_C> P_D$ and $P_{C1}< P_D$, the steady-state margin is P_{B1}.
- If $P_C > P_D$ and $P_{C1}>= P_D$, the steady-state margin is P_{C1}.

In this basic pattern, P_{B1} can never be the dynamic stability margin. Since P_{C1} and P_D are always less than P_{B1}, and C1 is the singularity-induced bifurcation point, the system cannot go beyond point C1. But when $P_C> P_D$ and $P_{C1}< P_D$, with load perturbation analysis, we know that the system can go beyond point D and will go to point B1, so P_{B1} is the steady-state margin. According to our experience, the scenario $P_C > P_D$ seldom occurs. In our study, it appears with a short transmission line, one that is less than 50 miles long.

Comparing Figure 6-13 to Figure 6-14 shows that x_d and E_{fd}_max in Figure 6-14 are larger than those in Figure 6-13, and the point D in Figure 6-14 is nearly at the same position as point B1 in Figure 6-13. This implies that larger exciter size is required for bigger x_d to keep same voltage stability margin for a given transmission line. Also, larger exciter size is required for longer transmission lines to keep same voltage stability margin for a given x_d.

Based on our analysis in section 6.3, we conclude that the situation $P_A(P_B) <P_D$ only occurs when the regulator is not well tuned (e.g., K_p is too small), or the transmission line is too long. In this case, dynamic analysis is necessary, and point A is the real stability margin because that P_A is always less than P_C. It is known that point A is mainly caused

by the regulator for a given transmission line, so the regulator is mainly responsible for the voltage collapse in this case. Steady-state analysis is no longer good enough in this case, as the real stability margin is determined by point A.

According to our experiences, situations $P_A>P_D$, $P_C>P_D$ and $P_{C1}<P_D$ are found in most cases (with a well-tuned regulator and transmission lines that are not too long). P_D is usually the real stability margin for the lower pattern, while P_{B1} is the real stability margin for the upper pattern. Both P_{B1} and P_D can be solved by the steady-state method. For these cases, steady-state analysis is good enough. Given a transmission line, P_D and P_{B1} are mainly determined by the exciter size; thus, the exciter should be mainly charged for the voltage collapse in this case.

6.5 The influence of the load pattern on the bifurcation points

In Chapter 1, we analyzed the influence of load pattern. Here we extend the study to bifurcation analysis, and show how different load patterns influence the PV curve and bifurcation points.

From Chapter 1, we know the load model can be expressed as:

$$P = P_0 (E/E_0)^{PE} * (\omega/\omega_0)^{Pf}$$

$$Q = Q_0 (E/E_0)^{QE} *(\omega/\omega_0)^{Qf}$$

$$Q_0 = \beta_0 P_0$$

Here we still assume that the voltage dynamic is decoupled from the angle dynamic, which is well behaved, so the angle dynamic can be ignored. Thus, in our analysis, we can assume that $\omega/\omega_0 \equiv 1$.

Now we will discuss how *PE*, *QE* and β impact voltage stability.

6.5.1 The influence of β_0

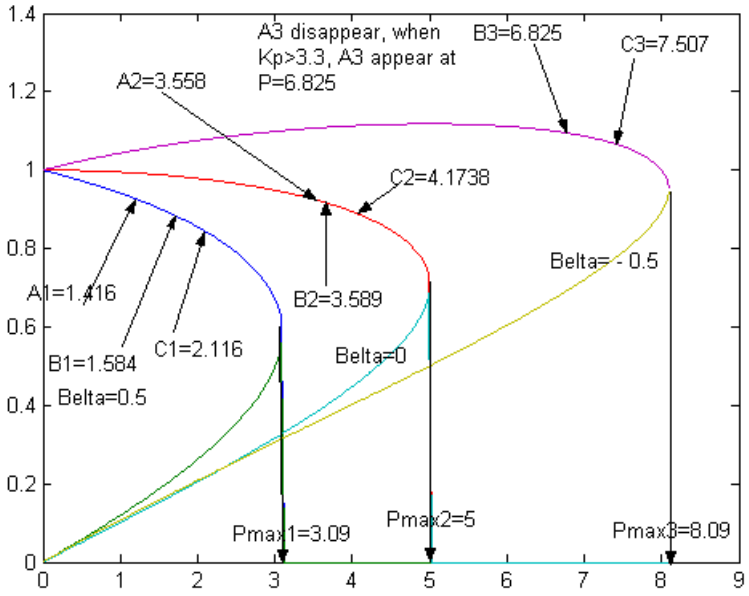

Figure 6-15 The influence of β_0

In Figure 6-15, there are three PV curves in which all load pattern are constant load, β_0 equals to 0.5, 0 and –0.5 respectively; the other conditions are kept as same. We see that β_0 has a big influence on the dynamic and static stability margins, and we have a bigger Pmax and stability margin with smaller β_0.

6.5.2 The influence of PE and QE on Pmax

We define $\beta = \frac{Q}{P} = \frac{Q_0 E^{QE}}{P_0 E^{PE}} = \beta_0 E^{QE-PE}$; it corresponds to the power factor of the load.

When β_0=0, it is apparent that $\beta = \beta_0$, *PE* and *QE* will have no influence on the Pmax.

When β_0>0,

If QE>PE, E^{QE-PE}<1, so $\beta < \beta_0$, we have bigger Pmax than constant load;
If QE<PE, E^{QE-PE}>1, so $\beta > \beta_0$, we have smaller Pmax than constant load; and
If QE=PE, E^{QE-PE}=1, so $\beta = \beta_0$, we have the same Pmax as constant load.

When β_0<0,

If QE>PE, E^{QE-PE}<1, so $\beta > \beta_0$, we have smaller Pmax than constant load;

If QE<PE, E^{QE-PE} >1, so $\beta < \beta_0$, we have bigger Pmax than constant load; and

If QE=PE, E^{QE-PE} =1, so $\beta = \beta_0$, we have the same Pmax as constant load.

Example:

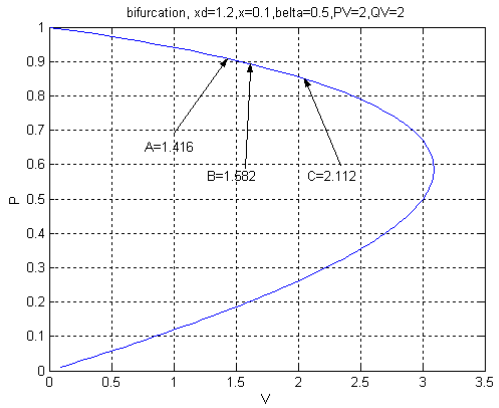

Figure 6-16 Bifurcation point locations on PV curve with load parameters β_0 =0.5, PE=0, and QE=0

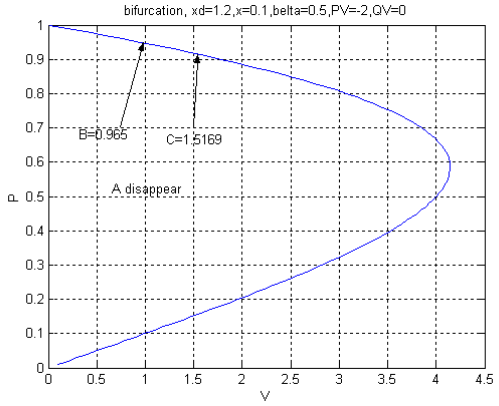

Figure 6-17 Bifurcation point locations on PV curve with load parameters β_0 =0.5, PE=-2, and QE=0

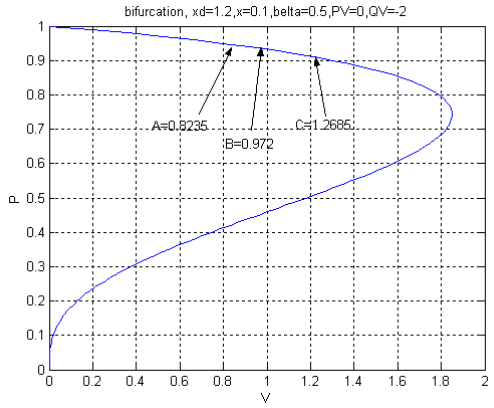

Figure 6-18 Bifurcation point locations on PV curve with load parameters β_0=0.5, PE=0, and QE=-2

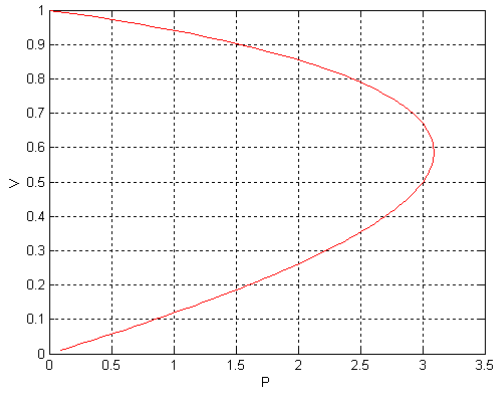

Figure 6-19 Bifurcation point locations on PV curve with load parameters β_0=0.5, PE=2, and QE=2

Comparing Figures 6-16 and 6-17, we see that when β_0>0, and QE>PE, we have bigger Pmax than constant load.

Comparing Figures 6-16 and 6-18, we see that when β_0>0, and QE<PE, we have smaller Pmax than constant load.

Comparing Figures 6-16 and 6-19, we see that when β_0>0, and QE=PE, we have the same Pmax as constant load.

6.5.3 The influence of *PE* and *QE* on bifurcation points

6.5.3.1 The influence of *PE* and *QE* on singular point C

For the described load above, there is no singular point C when $\beta_0 = 0$ and $PE \geq 1$. This can be easily derived from the following equations.

g: $0 = E'^2 E^2 - (x'P)^2 - (x'Q + E^2)^2$, (6-18)

$P = P_0 E^{PE}$, $Q = Q_0 E^{QE}$, $Q_0 = \beta_0 P_0$ (6-19)

Examples:

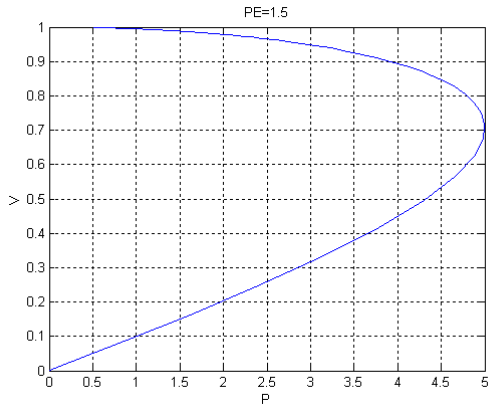

Figure 6-20 No bifurcation point locations on PV curve with lighting load

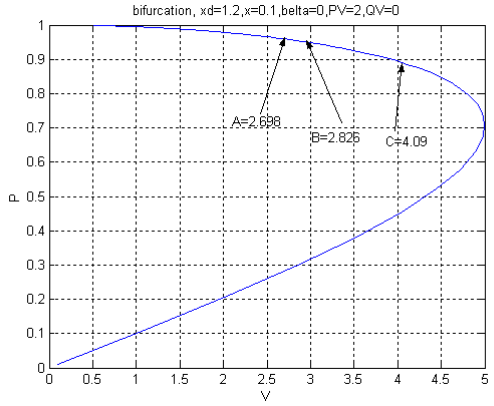

Figure 6-21 Bifurcation point locations on PV curve with constant load

Comparing Figure 6-20 to Figure 6-21, we see that there is no singular point when β_0=0 and $PE \geq 1$, but when β_0=0 and $PE < 1$, singular point C will appear.

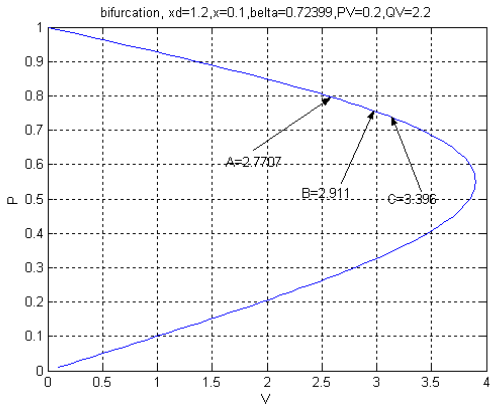

Figure 6-22 Bifurcation point locations on PV curve with central a/c type load

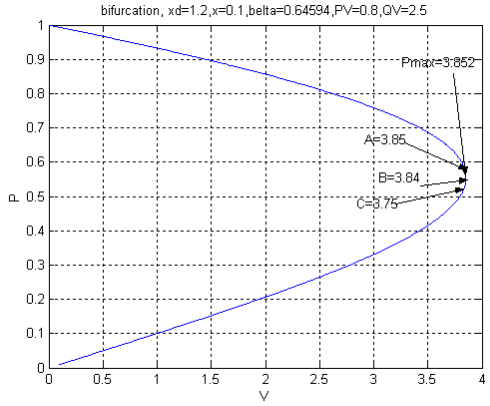

Figure 6-23 Bifurcation point locations on PV Curve with refrigerator type load

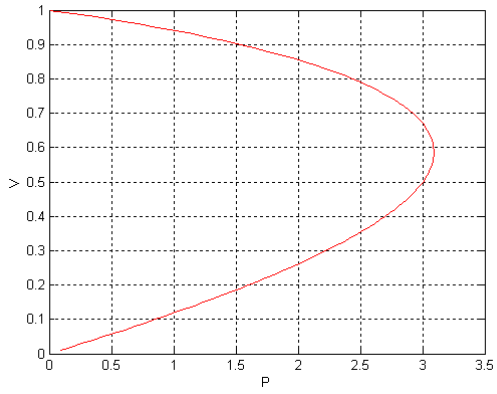

Figure 6-24 No bifurcation point locations on PV curve with constant resistance load

For central A/C, PE=0.2, Pf=0.9, QE=2.2, Qf = -2.7, β_0 =0.724.

For refrigerator, PE=0.8, Pf=0.5, QE=2.5, Qf=-1.4, β_0 = 0.6459.

For impedance load in Figure 6-24, PE=2, Pf=0, QE=2, Qf=0, β_0 = 0.5.

6.5.3.2 The influence of *PE* and *QE* on other bifurcation points

Based on our observation on the simple two-bus system, we found that with bigger PE, A, B and C points go further down to Pmax. Therefore, we have a larger stability margin. When β_0 >0, with larger QE, A, B and C points go further down to Pmax, so we can have a larger stability margin. However, when β_0 <0, with smaller QE, A, B and C points go further down to Pmax, which also means that we have a larger stability margin. It is apparent that QE will have no influence when β_0 =0.

Examples:

Comparing Figure 6-16 to Figure 6-17, we see that with a larger PE in Figure 6-16, there is a larger stability margin than in Figure 6-17. Comparing Figure 6-16 to Figure 6-18, we see that when β_0 >0, with a bigger QE in Figure 6-16, there is a larger stability margin than in Figure 6-18.

6.6 Publications

For the allocation of the responsibility/ contribution of the voltage stability, reader can refer to the paper in reference [6].

7
Conclusions

The phenomenon of voltage stability within the context of an increasingly competitive power market environment has been explored in this project. The effects of FACTS devices and types of load on voltage stability limits have been analyzed. Modeling issues for studying the effects of the various components have been discussed.

A voltage stability indicator has been analyzed to represent the phenomenon during a variety of control situations. The numerical simulation demonstrated the indicator's applicability.

The proposed voltage stability indicator has been explored for its applicability to detect a potential dynamic voltage collapse situation. Results from time-domain simulations using EUROSTAG, a commercial software product, has been used to compute the indicator. The importance of dynamic generation reserves on dynamic voltage stability has also been studied through time-domain simulations in this project. [8]

An algorithm to incorporate steady-state voltage stability into conventional optimal power flow formulation has been proposed. Incorporating FACTS devices and its application in composite reliability analysis was studied.

A transaction-based power flow procedure has been developed to effectively address the issue of equitable loss allocation and congestion management in a market environment. A new procedure to allocate voltage stability usage on a transaction basis has been proposed. We feel that this procedure has the potential to address utilization, responsibility settlement, security management and pricing from the voltage stability perspective.

Finally, a new way of using bifurcation analysis to allocate the contribution of generators, transmission and control elements has been proposed. The impacts of load patterns and exciter sizes on dynamic stability were also discussed. These analyses can help in allocating responsibility for a stability problem, and can also be of benefit in designing the system to avoid voltage collapse.

References

[1] G M Huang, N C Nair, “An OPF based Algorithm to Evaluate Load Curtailment Incorporating Voltage Stability Margin Criterion”, Conference proceeding of NAPS 2001, TX.

[2] G M Huang, N C Nair, “Voltage Stability Constrained Load Curtailment Procedure to Evaluate Power System Reliability Measures”, IEEE/PES WM 2002, NY.

[3] G M Huang, N C Nair, ”Incorporating TCSC into the Voltage Stability Constrained OPF Formulation”, IEEE/PES Summer meeting 2002, Chicago.

[4] G M Huang, N C Nair, “Detection of Dynamic Voltage Collapse”, IEEE/PES Summer meeting 2002, Chicago.

[5] G M Huang, N C Nair, “Allocating Usages of Voltage Security Margin in Deregulated Electric Markets”, ISCAS 2003, Thailand.

[6] G M Huang, K Men,” Contribution Allocation for Voltage Stability in Deregulated Power Systems”, IEEE 2002 PES, Summer meeting, Chicago.

[7] G M Huang, L Zhao, X Song, “A new bifurcation analysis for power system dynamic voltage stability studies”, IEEE 2002 PES, Summer Meeting, Chicago.

[8] G M Huang, H Zhang, “Dynamic voltage stability reserve studies for deregulated environment” IEEE 2001 PES, Summer Meeting, Canada

[9] G M Huang, H Zhang, “Transaction-Based Power Flow Analysis for Congestion Management and Responsibility Evaluation” presented at *2001 IEEE/PES Winter Meeting*, Panel Session: Transmission Congestion Management and Reliability, Columbus, Ohio.

[10] G M Huang, H Zhang, “Transaction-based Power Flow analysis For Transmission Utilization Allocation”, 2001 IEEE/PES Summer Meeting.

[11] G M Huang, H Zhang, “Transmission Loss Allocations and Pricing Via Bilateral Energy Transactions”, 1999 IEEE/PES Summer Meeting., Chicago, IL.

[12] V Venkatasubramanian, H Schaettler and J Zaborazky, "Voltage Dynamics: Study of a Generator with Voltage Control, Transmission, and Matched MW Load", IEEE Transactions on Automatic Control, Vol. 37, No.11, November 1992, pp. 1717-1733.

[13] Carson W Taylor, “Power System Voltage Stability”, McGraw-Hill, Inc., 1994.

[14] P Kessel, H Glavitsch, “Estimating the voltage stability of a power system”, IEEE Transactions on Power Delivery, Vol. PWRD-1, No.3, July 1986, pp. 346-354.